

Drought triggers and sustains overnight fires in North America

<https://doi.org/10.1038/s41586-024-07028-5>

Kaiwei Luo^{1✉}, Xianli Wang^{1,2✉}, Mark de Jong³ & Mike Flannigan^{1,4}

Received: 4 April 2023

Accepted: 4 January 2024

Published online: 13 March 2024

 Check for updates

Overnight fires are emerging in North America with previously unknown drivers and implications. This notable phenomenon challenges the traditional understanding of the ‘active day, quiet night’ model of the diurnal fire cycle^{1–3} and current fire management practices^{4,5}. Here we demonstrate that drought conditions promote overnight burning, which is a key mechanism fostering large active fires. We examined the hourly diurnal cycle of 23,557 fires and identified 1,095 overnight burning events (OBEs, each defined as a night when a fire burned through the night) in North America during 2017–2020 using geostationary satellite data and terrestrial fire records. A total of 99% of OBEs were associated with large fires (>1,000 ha) and at least one OBE was identified in 20% of these large fires. OBEs were early onset after ignition and OBE frequency was positively correlated with fire size. Although warming is weakening the climatological barrier to night-time fires⁶, we found that the main driver of recent OBEs in large fires was the accumulated fuel dryness and availability (that is, drought conditions), which tended to lead to consecutive OBEs in a single wildfire for several days and even weeks. Critically, we show that daytime drought indicators can predict whether an OBE will occur the following night, which could facilitate early detection and management of night-time fires. We also observed increases in fire weather conditions conducive to OBEs over recent decades, suggesting an accelerated disruption of the diurnal fire cycle.

Asymmetric warming, in which nights are warming more rapidly than days resulting from anthropogenic climate change^{7,8}, may markedly affect diurnal fire activity. Although changing daytime conditions⁹ are known to exacerbate fires⁹, the potential shifts in night-time burning have received less attention, as night-time fires are typically hindered by cooler and moister atmospheric conditions and increased moisture in fine fuels¹⁰. This conventional understanding of the day–night fire pattern has been widely applied to fire suppression⁴ and prescribed⁵, cultural¹ and agricultural^{2,3} burning. However, recent reports from frontline firefighters and satellite observations have indicated an increase in the frequency and duration of night-time fire incidents in Canada and the USA and an increase in the number and intensity of night-time fire ‘hotspots’^{6,11}. These findings raise concerns that increasing night-time flammability in certain regions may be expanding the diurnal burning period towards a tipping point, at which the absence of night-time conditions acting as a break on fire activity could lead to self-perpetuating overnight burning and thus larger, longer-duration fires.

Satellite-based active fire products provide consistent observations of fire activity over many years¹². However, existing research^{13–15} on fire diurnal cycles has primarily focused on regional-scale patterns, with fire extent and intensity often peaking in the mid-afternoon. Studies have shown that night-time fire seasons are shorter than daytime fire seasons in most Australian¹⁰ and global⁶ climate regions. Night-time

hotspots tend to be present during the peak fire season^{6,16} and are more commonly associated with large fires, especially in arid regions¹⁷ and under extreme droughts¹¹. Although local cases of overnight fire have been documented¹⁸, we were unable to find any methodical studies exploring this phenomenon and its implications or its underlying driving factors.

Fire activity has been widely linked to weather conditions captured by fire weather indices and meteorological parameters, such as the Canadian Fire Weather Index System (CFWIS)¹⁹ and vapour pressure deficit (VPD, a widely used metric measuring how rapidly the atmosphere dries fuel)²⁰. The CFWIS components are the most commonly used indices for both operational and research purposes regionally^{21,22} and globally^{23–25}. The CFWIS first tracks potential fuel moisture conditions in surface fine fuel and moderate and deep organic layers at daily or hourly time steps²⁶, capturing the varying speeds with which these fuels react to ambient weather. Using the resulting fuel moisture codes, the CFWIS then derives indices of potential fire behaviour: potential rate of spread, available fuel and fire intensity²⁷. The extent to which fires can burn at night is partly governed by diurnal weather fluctuations²⁸ and corresponding changes in small-diameter dead surface fuel moisture²⁹. The day–night extrema values and range of these factors can be important for overnight burning as they determine both the initial conditions at the start of the night and night-time minima, and a smaller day–night range may sustain

¹Department of Renewable Resources, University of Alberta, Edmonton, Alberta, Canada. ²Natural Resources Canada, Canadian Forest Service, Northern Forestry Centre, Edmonton, Alberta, Canada. ³Natural Resources Canada, Canadian Forest Service, Great Lakes Forestry Centre, Sault Ste. Marie, Ontario, Canada. ⁴Department of Natural Resource Science, Faculty of Science, Thompson Rivers University, Kamloops, British Columbia, Canada. ✉e-mail: kaiwei@ualberta.ca; xianli.wang@nrcan-rcan.gc.ca

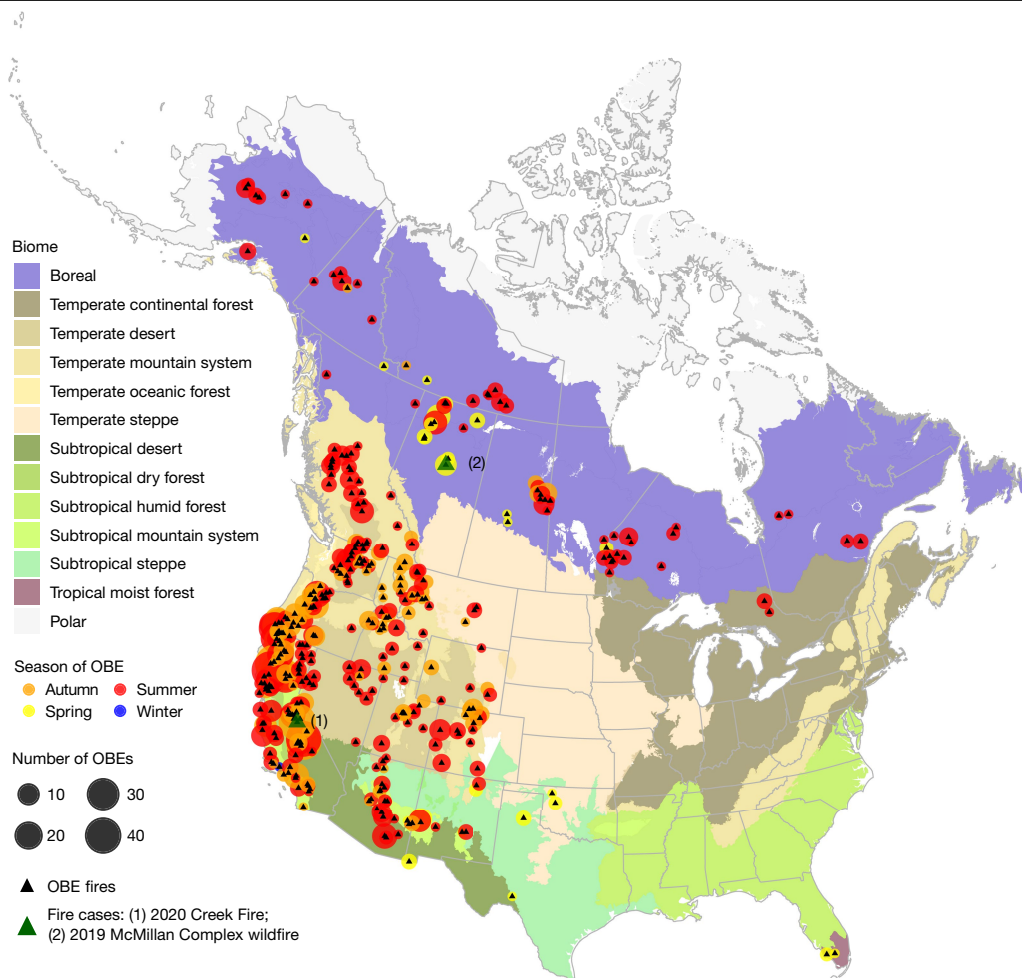


Fig. 1 | Substantial overnight burning in North America, 2017–2020. The map shows the season (such as summer: June–August) and the number of OBEs per OBE fire, which are represented by the colour and size of filled circles, respectively. When OBEs within a fire occur in several seasons, the geographic position is jittered and plotted several times with different colours for clearer visualization. The background is coloured by biome classifications. All OBE fires are represented by black triangles. A total of 1,095 OBEs were identified in 340 out of 23,557 fires and 99% of OBEs were associated with large fires

(>1,000 ha). Among these large fires, 20% were OBE fires. OBEs were mostly concentrated in western mountain areas and the boreal region. Multi-OBE fires were the predominant form of OBE fires and accounted for 85% of all OBEs, with the top 10 multi-OBE fires averaging 27.1 nights of overnight burning. The numbered green triangles represent two large fire cases that are discussed further: (1) the 2020 Creek Fire (California, subtropical mountain system) and (2) the 2019 McMillan Complex wildfire (Alberta, boreal region). The identification approach for OBEs can be found in the Methods.

longer-lasting night-time burning. Large-diameter dead surface fuels and subsurface soil and organic materials that react slowly to meteorological conditions may also play a key role in overnight burning as they provide relatively stable influences on fires^{11,30}, despite diurnal meteorological fluctuations. The systematic effect of slow-reacting and fast-reacting fuels and weather dynamics on overnight burning remains unexplored.

Here we combined high-temporal-resolution active fire data from the Geostationary Operational Environmental Satellite-R (GOES-R) Series³¹ with high-spatial-resolution terrestrial fire datasets to characterize the hourly fire diurnal cycle of each fire and identify OBEs (overnight burning events, defined as nights when fires burned through the entire night) in North America during the period 2017–2020 (Methods and Extended Data Fig. 1). The distribution, characteristics and implications of OBE fires (that is, fires with at least one OBE) were examined in detail. A systematic examination of fire weather metrics (including CFWIS and VPD) based on the European Centre for Medium-Range Weather Forecasts Reanalysis version 5 (ERA5)³² was conducted to assess underlying drivers and explore the prediction of OBEs. This study represents a comprehensive exploration of the overnight burning

phenomenon, including its characteristics, implications, underlying drivers and prediction. It will contribute to the knowledge gap in diurnal fire activity and its changing nature, and has practical implications for night-time fire management.

Widespread and extreme overnight burning

We studied the diurnal cycles of 23,557 fires that occurred in North America during 2017–2020 and a total of 1,095 OBEs were identified in 340 fires (Fig. 1 and Extended Data Table 1). OBEs were rare in small fires but common in large fires. Out of a total of 21,116 fires smaller than 1,000 ha, only 11 OBEs were identified (Extended Data Fig. 2). Large fires (>1,000 ha) accounted for the remaining 99% of OBEs ($n = 1,084$), which constituted 2.2% of the total nights for these large fires. Among these large fires, 20% were OBE fires, with this proportion rising as high as 35% in western mountain areas. OBEs were mostly concentrated in western mountain areas (temperate mountain system: 45% and subtropical mountain system: 31%) and the boreal region (13%), in which large fires were also the most prevalent. OBEs peaked in summer (June–August) and autumn (September–November) in western mountain areas, with

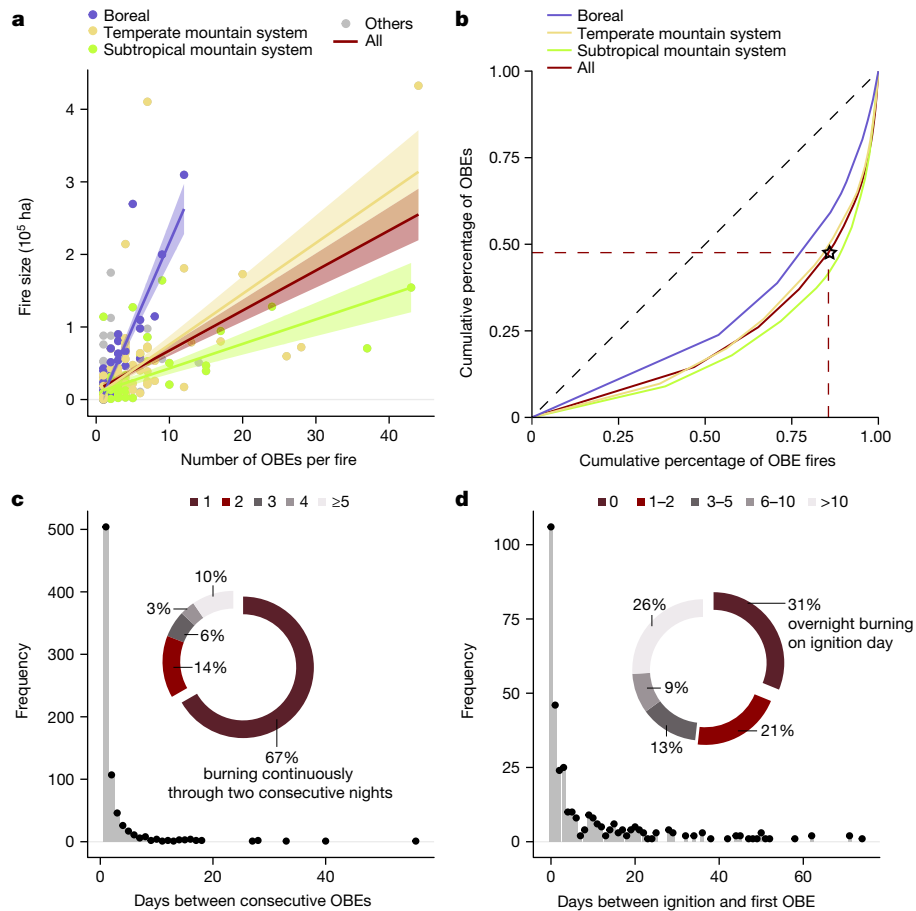


Fig. 2 | Overnight burning promotes extreme fires. a, Fire size versus the number of OBEs per OBE fire by biome and for all biomes combined ('All'). Relationships are fitted using linear regression and, in all cases, $P < 0.05$, indicating that fire size is positively correlated to the number of OBEs. The shaded area surrounding the line represents the uncertainty ranges of the 95% confidence interval. **b**, Cumulative percentage of OBE fires versus cumulative percentage of OBEs by biome and for all biomes combined ('All'). The cumulative percentage of OBE fires is ordered by the number of OBEs, with single-OBE fires starting at 0% and fires with the highest number of OBEs at 100%. Dashed red lines indicate that 14% of OBE fires contributed to more

than half of all OBEs. **c**, The frequency and distribution of the number of days between each OBE and the successive OBE in multi-OBE fires. In 67% of cases, OBEs occurred on two consecutive nights, indicating a frequent consecutive occurrence of OBEs. **d**, The frequency and distribution of the number of days between fire ignition and the occurrence of the first OBE, for all OBE fires. In 52% of OBE fires, the first OBE occurred within 2 days of ignition and in 31% of OBE fires, an OBE occurred on the ignition day. For better visualization, the only OBE fire (1 out of 340 OBE fires) with a time interval after ignition exceeding 100 days was excluded from the bar chart but included in the pie chart.

few in spring (March–May), whereas around a quarter of OBEs in the boreal region occurred in spring, especially in Alberta (Fig. 1).

Overnight burning potentially promotes extreme fires with larger burned areas and longer durations of active burning. We found a positive correlation between fire size and the number of OBEs (Fig. 2a). Notably, fires larger than 1,000 ha, although comprising only 10% of all fires, were responsible for 90% of the total area burned in North America during 2017–2020 based on the fire datasets analysed herein (Methods). Moreover, OBEs tend to occur consecutively. Multi-OBE fires (fires with more than one OBE) were the predominant form of OBE fires and accounted for 85% of all OBEs (Fig. 1 and Extended Data Table 1). More than 50% of OBEs were concentrated in just 14% of OBE fires (Fig. 2b), with the top 10 multi-OBE fires averaging 27.1 nights of overnight burning (Fig. 1). About two-thirds (63% and 62%, respectively) of OBE fires were multi-OBE fires in temperate and subtropical mountain systems, which actively burned through 5.4 and 6.4 nights on average, respectively (Extended Data Table 1). Calculating the number of days between two successive OBEs in each multi-OBE fire indicated that most OBEs are temporally clustered, often occurring continuously or within a short time interval during the lifetime of a fire (Fig. 2c). For example, 43 OBEs were identified within 52 days of the Creek Fire in

California during the 2020 fire season (Fig. 1 and Extended Data Fig. 3), resulting in a total area burned exceeding 150,000 ha. Furthermore, the first OBE of all OBE fires tended to occur in the first few days after ignition; more than 50% of the first OBEs occurred within 2 days of ignition and nearly one-third of the first OBEs occurred on the day of ignition (Fig. 2d). This leaves little time for firefighting interventions, which—combined with the consecutive occurrence of OBEs—increases the likelihood of OBE fires becoming out of control and reaching large final sizes.

We used Earth Observation fire products from the GOES-R geostationary satellite series as it is the only source of regular, high-frequency fire detections (≤ 15 -min temporal resolution) for North America and is, therefore, the only satellite system capable of identifying OBEs (Methods). Notably, the number and characteristics of OBEs and OBE fires reported herein are still likely to be conservatively estimated, given our stringent requirements for identifying an OBE (Methods) and the omission errors of Earth-observation-based active fire detection algorithms (for example, cloud/vegetation canopy obscuration, oblique sensor observation angles and small and/or smouldering fires with limited fire extents and intensities that fall below the minimum detection thresholds)³³.

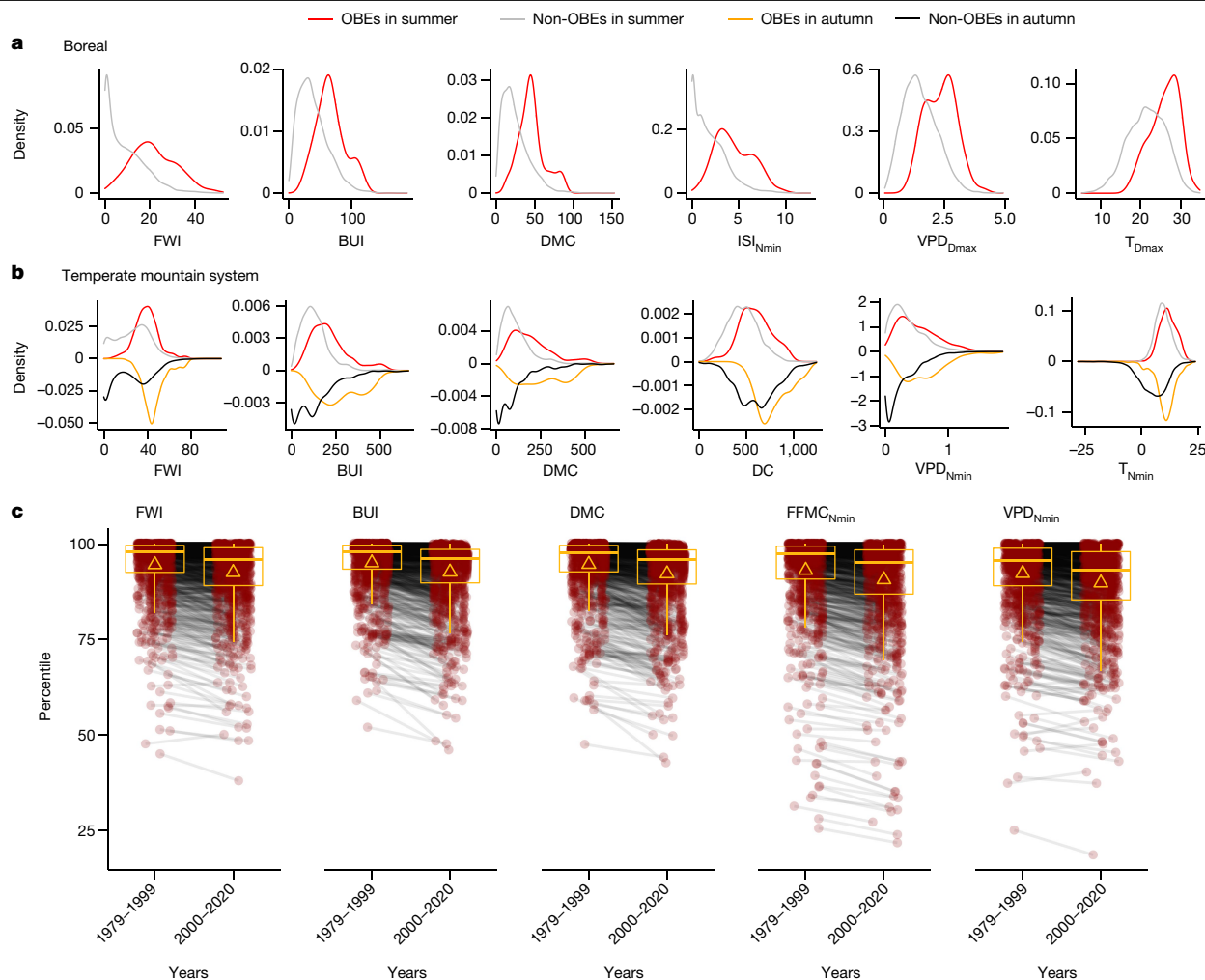


Fig. 3 | Fire weather is elevated during overnight burning and has become more extreme over time. a, b, Significantly greater (one-sided Mann–Whitney *U* test, $P < 0.05$) fire weather conditions for OBEs (red for summer and orange for autumn) than those for non-OBEs (grey for summer and black for autumn) within fires larger than 1,000 ha in the boreal (a) and temperate mountain system (b). We invert the y-axis of these distributions in autumn for clearer visualization. Details for all variables in the five main biome–season groups are shown in Extended Data Fig. 4. **c,** The line-linked paired points respectively represent the percentile of fire weather for each OBE within fires larger than

1,000 ha relative to comparable observations during the 1979–1999 and 2000–2020 periods at the same geographic location. The 1979–1999 percentiles are significantly higher than the 2000–2020 percentiles for each fire weather variable (paired Wilcoxon test, $P < 0.05$), indicating an increasing trend in fire weather conditions conducive to overnight burning in recent decades. Box plots show the distribution of these percentile values, with a median line, mean triangle and box ends representing first and third quartiles. Whiskers extend to values within 1.5 times the interquartile range. Details for other fire weather variables are shown in Extended Data Fig. 6.

Drought drives overnight burning

Given that 99% of OBEs were detected in fires larger than 1,000 ha, we focused our analysis on these large fires to investigate the underlying factors contributing to OBEs. We examined the differences in all fire weather variables (including daily slow-reacting variables and the day-time and night-time extrema values of hourly fast-reacting variables), as well as the day–night range of fast-reacting variables, between OBEs and non-OBEs within fires larger than 1,000 ha (Methods). We focused on this analysis in the five main biome–season groups with 100 or more OBEs, which included boreal summer, temperate mountain system summer and autumn, and subtropical mountain system summer and autumn (Extended Data Table 1). Substantially hotter, drier and windier conditions were found for OBEs compared with non-OBEs as almost all fire weather variables showed significantly lower (relative humidity) and higher (other variables) values for OBEs (one-sided Mann–Whitney *U* test, $P < 0.05$; Fig. 3a,b and Extended Data Fig. 4). For example, in the temperate mountain system autumn, the mean value of moderately slow-drying fuel moisture (DMC, 255.8) and potential fuel availability

(BUI, 279.3) for OBEs were, respectively, 152% and 116% higher than non-OBEs (101.6 and 129.1, respectively). However, the day–night ranges of all fast-reacting weather variables for OBEs were not significantly smaller than for non-OBEs (Extended Data Fig. 5).

Moreover, to assess the fire weather extremes for OBEs, we calculated the percentile value of each OBE’s fire weather variable from fires larger than 1,000 ha relative to the distribution of values extracted from records for the years 2000–2020 and 1979–1999 in the corresponding fire perimeter. The value of each fire weather variable for OBEs generally exceeded the 90th percentile of comparable observations during 2000–2020 in the same location (Fig. 3c and Extended Data Fig. 6), for example, BUI and DMC exceeded the 93rd and 92nd percentiles, respectively. Extreme fire weather conditions were indicative of potentially high burning intensity (FWI) and fire spread (ISI). Days and nights associated with OBEs were prone to becoming ‘fire spread days’, characterized by substantial area growth³⁴, leading to large fire sizes. Notably, for OBEs, co-located fire weather percentiles calculated on the basis of the 2000–2020 climatology were significantly lower (paired Wilcoxon test) than those calculated on the basis of the

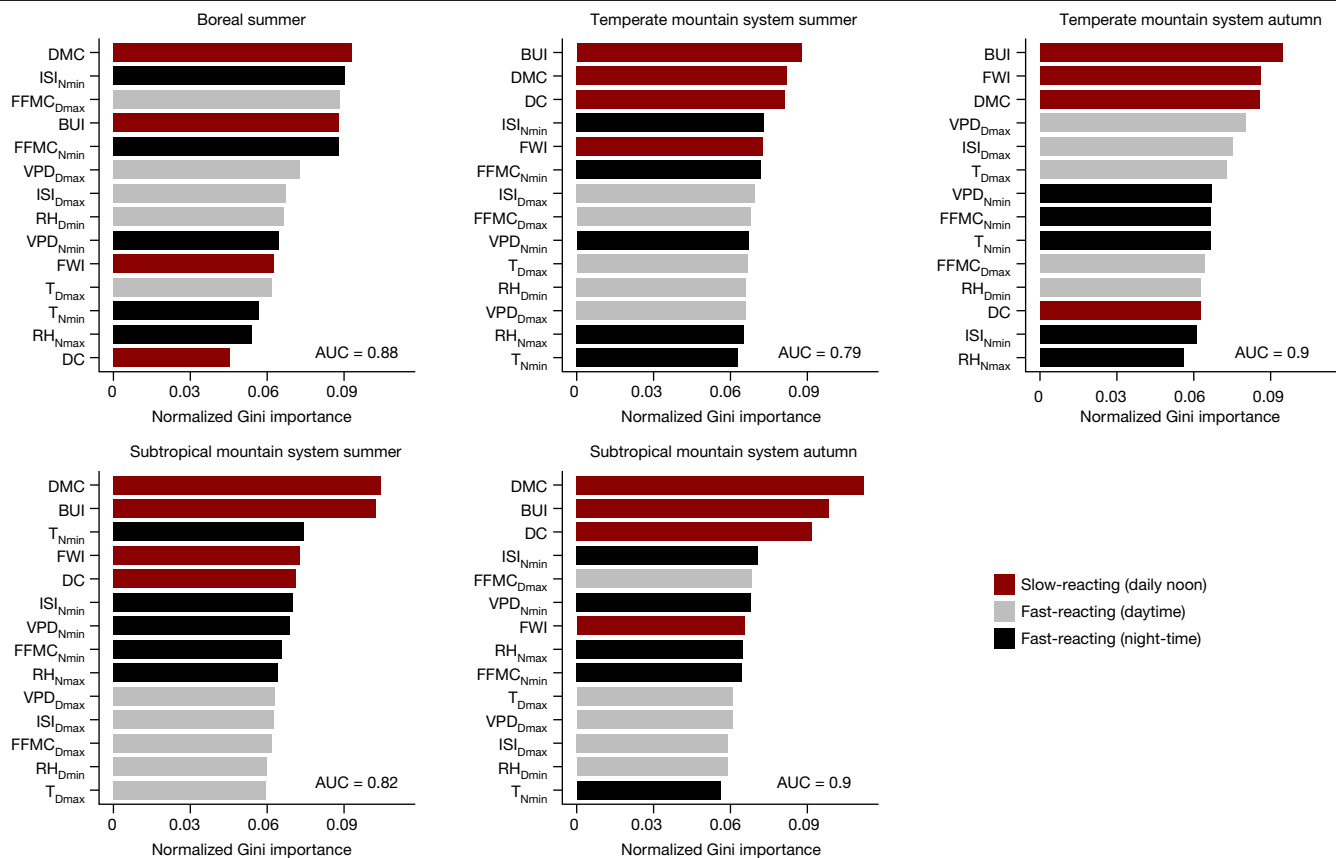


Fig. 4 | Drought conditions are the main driver of overnight burning. For each main biome–season group, we calculate the normalized mean decreases in the Gini coefficient of fire weather variables using the random forest model to classify OBEs or non-OBEs for nights of fires larger than 1,000 ha. The variables are ranked from the most important to the least important. Slow-reacting variables are represented by dark-red horizontal bars and daytime

and night-time extrema of fast-reacting variables by grey and black bars, respectively. Drought conditions play a crucial role in supporting OBEs as either DMC or BUI (cumulative fuel dryness or amount; drought-related variables) was found to be the most important factor in all groups. The performance of the models is evaluated by the area under the receiver operating characteristic curve (AUC).

1979–1999 climatology (Fig. 3c), indicating an increasing trend in fire weather conditions conducive to overnight burning in recent decades.

To further understand the underlying drivers of recent OBEs, we constructed random forest binary classification (that is, OBEs or non-OBEs) models³⁵ for nights of fires larger than 1,000 ha in the five main biome–season groups to determine the relative importance of fire weather variables (Methods). We excluded ranges of fast-reacting variables in this analysis because of their insignificance in the previous analysis (Extended Data Fig. 5). The results indicated that cumulative fuel dryness and amount (that is, drought-related variables) played a crucial role in supporting OBEs (Fig. 4). Specifically, either DMC or BUI was found to be the most important factor in all groups. Moreover, further analysis that included all OBEs from all fire sizes (Extended Data Fig. 7) and the qualitative analysis of the 2020 Creek Fire in California (Extended Data Fig. 3) also illustrated the dominant role of drought conditions on OBEs. Notably, despite the dominance of drought, surface fine fuel moisture (FFMC) and potential fire spread (ISI) also strongly influenced OBEs in boreal summer and temperate mountain system summer.

Overnight burning is predictable

In operational wildfire management, fire danger indices and adjective ratings used for decision-making are typically generated at a daily (that is, local noon) time step, rather than an hourly one, especially in remote areas³⁶. To explore the potential predictability of OBEs (that is, whether the coming night is an OBE or not) in such an operational setting and to

understand the coupling between daytime conditions and night-time burning, we constructed logistic regression models (Methods) for nights of fires larger than 1,000 ha in five main biome–season groups using different combinations of daily-noon slow-reacting variables given the importance of these variables (Fig. 4). The results indicated that OBEs were predictable and that daytime conditions largely set the foundation for their occurrence. For each biome–season group, at least 66% of OBEs were correctly predicted (Extended Data Table 2). For example, in the best-performing model for the temperate mountain system autumn, 82.6% of OBEs were correctly predicted (Fig. 5).

Overnight fires are an emerging challenge

Compared with interannual, annual and seasonal fire activity, diurnal fire activity—especially the night-time aspect—has long been overlooked. However, the recent widespread occurrence of unexpected and extreme OBEs in conventional large-fire-prone areas in North America has highlighted the urgency of this research. 99% of OBEs were associated with large fires (>1,000 ha) and at least one OBE was identified in 20% of these large fires. OBEs were early onset after ignition (>50% of the first OBE of all OBE fires occurred within 2 days of ignition) and OBE frequency was positively correlated with fire size. These findings combined with the frequent consecutive occurrence of OBEs are challenging traditional diurnal fire knowledge and current fire management practices. The occurrences of OBEs are associated with extreme fire weather, particularly intensified fuel dryness and availability (that is, drought conditions). Drought conditions disrupt the usual balance of

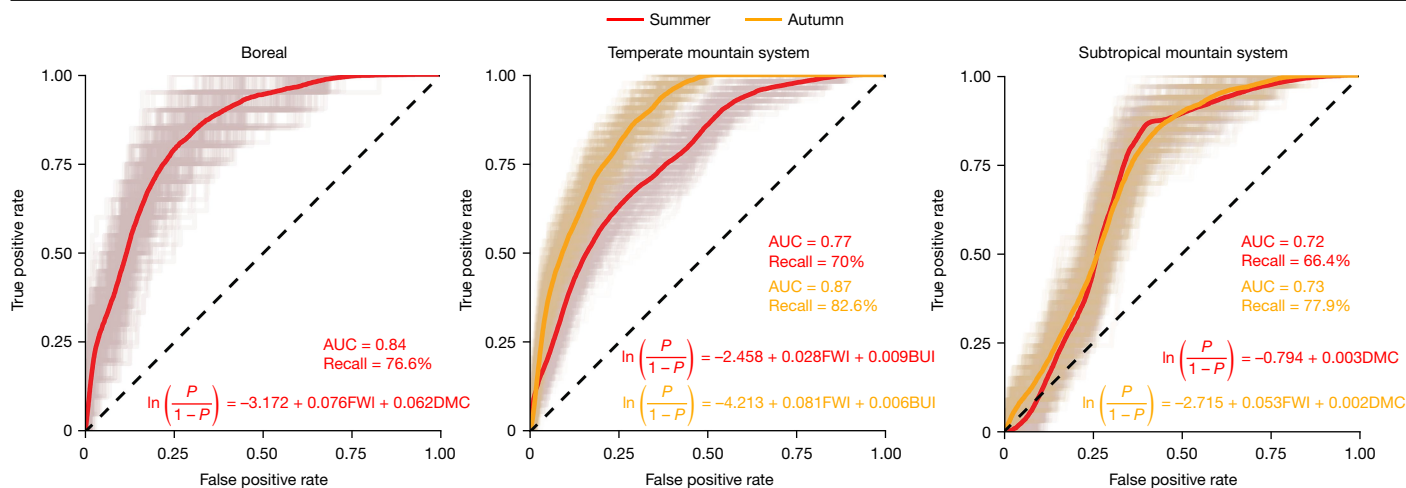


Fig. 5 | Overnight burning is predictable based on daytime fire weather conditions. Logistic regression models were built to predict whether nights of fires larger than 1,000 ha were OBEs or non-OBEs in each main biome–season group, using daily fire weather variables only. The receiver operator characterization curve (ROC) of each resample (background pale lines) for a 50 times fivefold cross-validation and the ROC from all resamples (coloured lines) are shown in each subplot, with the overall area under the ROC (AUC) value presented. The recall represents the percentage of correctly predicted OBEs

diurnal flammability and promote overnight burning, which is a key mechanism fostering large active fires. Our study also emphasizes the predictability of OBEs with daily-noon conditions, providing new insights into the diurnal fire cycle, with implications for night-time fire management.

Overnight burning presents substantial challenges for fire management. First, conditions conducive to OBEs typically occur when fire suppression capacity is already stretched. The extended burning duration, larger burned area and intensity and extreme fire behaviour can exponentially increase containment expenses³⁷. Second, the early onset of OBEs after ignition leaves little time for firefighters to react and the consecutive occurrence of OBEs limits containment options. Multi-OBE fires, the dominant form of overnight burning, are therefore harder to suppress and more likely to become escaped fires. Third, firefighters face limited time for rehydration, sleep and reduced body temperature, exacerbating physical and mental stress³⁸. Reduced visibility and more complicated night-time situations further escalate this adversity^{11,39}. To cope with these challenges, early fire detection efforts and developing new tools that allow for more effective decision-making may be beneficial given the increasing budget pressures on fire management⁴⁰. For example, as we show here for the first time, OBEs are predictable based on daytime conditions. Combining these findings with fire weather forecasting and real-time data assimilation of observations in an operational system could enhance strategic and tactical fire management decisions.

We identified that the main drivers of OBEs were cumulative fuel dryness and availability, which aligns with previous studies that have suggested that night-time fires (for example, higher occurrence¹⁷ and longer persistence^{11,18}) favour drier conditions. These factors not only react slowly to diurnal fluctuations but also exhibit time lags of days to weeks¹⁹, which prevent fires from being extinguished during adverse night-time conditions. This may also explain why OBEs usually occur on consecutive or nearly consecutive nights (Fig. 2c). Nonetheless, the drivers of OBEs may still vary between regions and seasons, and the role of fast-reacting variables should not be discounted. For instance, nearly a quarter of boreal OBEs were identified in spring when fuel dryness and availability usually cannot accumulate sufficiently. The qualitative analysis of the 2019 McMillan Complex wildfire, Alberta

among observed OBEs. The equations in each subplot show the logistic equations for the model output in different biomes, in which P represents the probability of OBE occurrence. At least 66% of OBEs were correctly predicted for each group, indicating that OBEs are predictable and that daytime conditions largely set the foundation for their occurrence. The overall ROC, AUC, recall and logistic equations are coloured by season, that is, red for summer and orange for autumn.

(Extended Data Fig. 8) and previous research on large spring fires in Alberta⁴¹ indicate that wind may play an important role in spring OBEs in the boreal region. Sudden changes in night-time conditions, such as the passage of a dry cold front⁴² or the onset of heatwave conditions, can also weaken or even eliminate the night-time barrier to fires, resulting in OBEs. As well as their role in promoting OBEs, the importance of fast-reacting variables also lies in the fact that they can inhibit overnight burning. For instance, even when drought indicators have accumulated to high levels, these fast-reacting variables can interrupt the consecutive occurrence of OBEs, as demonstrated in the qualitative analysis of the 2020 Creek Fire (Extended Data Fig. 3). It is also worth noting that cumulative fuel dryness and availability are primarily induced by prolonged periods of insufficient precipitation and high temperatures, further underscoring the significance of fast-reacting variables. Furthermore, as large fires are typically associated with drought conditions⁴³, a potential consequence of the detection limits of the GOES-R active fire product is an increased emphasis on the role of variables that reflect fuel dryness and availability.

We have found a rise in extreme fire weather conditions conducive to OBEs in recent decades, which is consistent with the prolonged drying period (for example, extreme droughts in the western USA)^{44,45} and increasing trends in fire-conductive weather during the day or night^{6,7,46}. However, the relationship between diurnal fire activity and climate change remains largely understudied. First, as climate change drives the transition to flash, intensified and prolonged droughts⁴⁷, it is expected to compress the time frame in which factors leading to OBEs accumulate. This could potentially result in a future scenario in which OBEs occur more rapidly since onset of fire and occur more frequently in succession, posing much greater challenges for mitigation and management. Second, warming is eroding the climatological barrier that traditionally restricted night-time fires⁶. The asymmetric increasing trend in fast-reacting variables, such as temperature and VPD, therefore holds the potential to drive broader shifts in diurnal burning patterns, leading to an increased occurrence of OBEs that may rely less on drought conditions. The nonlinear impact of asymmetric warming, in which a slight increase in daytime temperatures may disproportionately enhance diurnal flammability, adds an extra layer of complexity to this issue. To gain a deeper understanding of

this complex relationship, future research should involve the examination of both fuel and climatological factors evaluated in an integrated day–night manner. It may also be beneficial to combine active fire observations from both low-Earth-orbit and geostationary platforms to improve OBE detection and understanding of the diurnal fire cycle. Furthermore, insights into how diurnal burning patterns are expected to shift regionally and globally in the future can provide both scientific and practical value for confronting future fire challenges^{48,49}.

Online content

Any methods, additional references, Nature Portfolio reporting summaries, source data, extended data, supplementary information, acknowledgements, peer review information; details of author contributions and competing interests; and statements of data and code availability are available at <https://doi.org/10.1038/s41586-024-07028-5>.

- Pyne, S. J. *Fire in America: A Cultural History of Wildland and Rural Fire* (Univ. Washington Press, 2017).
- Zhang, T., Wooster, M. J. & Xu, W. Approaches for synergistically exploiting VIIRS I- and M-Band data in regional active fire detection and FRP assessment: a demonstration with respect to agricultural residue burning in Eastern China. *Remote Sens. Environ.* **198**, 407–424 (2017).
- Vadrevu, K. P., Ellicott, E., Badarinath, K. & Vermote, E. MODIS derived fire characteristics and aerosol optical depth variations during the agricultural residue burning season, north India. *Environ. Pollut.* **159**, 1560–1569 (2011).
- McHugh, C. W. & Gleason, P. in *Hayman Fire Case Study* General Technical Report RMRS-GTR-114 (ed. Graham, R. T.) 131–144 (USDA Forest Service, 2003).
- Arno, S. F. in *Wildland Fire in Ecosystems: Effects of Fire on Flora* General Technical Report RMRS-GTR-42-vol 2 (eds Brown, J. K. & Smith, J. K.) 97–120 (USDA Forest Service, 2000).
- Balch, J. K. et al. Warming weakens the night-time barrier to global fire. *Nature* **602**, 442–448 (2022).
- Chiodi, A. M., Potter, B. E. & Larkin, N. K. Multi-decadal change in western US nighttime vapor pressure deficit. *Geophys. Res. Lett.* **48**, e2021GL092830 (2021).
- Davy, R., Esau, I., Chernokulsky, A., Outten, S. & Zilitinkevich, S. Diurnal asymmetry to the observed global warming. *Int. J. Climatol.* **37**, 79–93 (2017).
- Jain, P., Castellanos-Acuna, D., Coogan, S. C., Abatzoglou, J. T. & Flannigan, M. D. Observed increases in extreme fire weather driven by atmospheric humidity and temperature. *Nat. Clim. Change* **12**, 63–70 (2022).
- Williamson, G. J. et al. Measurement of inter- and intra-annual variability of landscape fire activity at a continental scale: the Australian case. *Environ. Res. Lett.* **11**, 035003 (2016).
- Freeborn, P. H., Jolly, W. M., Cochrane, M. A. & Roberts, G. Large wildfire driven increases in nighttime fire activity observed across CONUS from 2003–2020. *Remote Sens. Environ.* **268**, 112777 (2022).
- Giglio, L., Csiszar, I. & Justice, C. O. Global distribution and seasonality of active fires as observed with the Terra and Aqua Moderate Resolution Imaging Spectroradiometer (MODIS) sensors. *J. Geophys. Res. Biogeosci.* **111**, G02016 (2006).
- Giglio, L. Characterization of the tropical diurnal fire cycle using VIRS and MODIS observations. *Remote Sens. Environ.* **108**, 407–421 (2007).
- Roberts, G., Wooster, M. & Lagoudakis, E. Annual and diurnal African biomass burning temporal dynamics. *Biogeosciences* **6**, 849–866 (2009).
- Amraoui, M., DaCamara, C. & Pereira, J. Detection and monitoring of African vegetation fires using MSG-SEVIRI imagery. *Remote Sens. Environ.* **114**, 1038–1052 (2010).
- Maier, S. W. & Russell-Smith, J. in *Flammable Australia: Fire Regimes, Biodiversity and Ecosystems in a Changing World* (eds Bradstock, R. A. et al.) 79–95 (CSIRO Publishing, 2012).
- Andela, N., Kaiser, J., van der Werf, G. & Wooster, M. New fire diurnal cycle characterizations to improve fire radiative energy assessments made from MODIS observations. *Atmos. Chem. Phys.* **15**, 8831–8846 (2015).
- Balch, J. K. et al. The susceptibility of southeastern Amazon forests to fire: insights from a large-scale burn experiment. *Bioscience* **65**, 893–905 (2015).
- Van Wagner, C. E. *Development and Structure of the Canadian Forest Fire Weather Index System* (Canadian Forestry Service, 1987).
- Veraverbeke, S. et al. Lightning as a major driver of recent large fire years in North American boreal forests. *Nat. Clim. Change* **7**, 529–534 (2017).
- Wang, X., Swystun, T. & Flannigan, M. D. Future wildfire extent and frequency determined by the longest fire-conductive weather spell. *Sci. Total Environ.* **830**, 154752 (2022).
- Groot, W. J. D., Field, R. D., Brady, M. A., Roswintarti, O. & Mohamad, M. Development of the Indonesian and Malaysian fire danger rating systems. *Mitig. Adapt. Strateg. Glob. Change* **12**, 165–180 (2007).
- Abatzoglou, J. T., Williams, A. P., Boschetti, L., Zubkova, M. & Kolden, C. A. Global patterns of interannual climate–fire relationships. *Glob. Change Biol.* **24**, 5164–5175 (2018).
- Jolly, W. M. et al. Climate-induced variations in global wildfire danger from 1979 to 2013. *Nat. Commun.* **6**, 7537 (2015).
- Di Giuseppe, F. et al. The potential predictability of fire danger provided by numerical weather prediction. *J. Appl. Meteorol. Climatol.* **55**, 2469–2491 (2016).
- Wotton, B. M. in *Proc. Eighth Symposium on Fire and Forest Meteorology* 13–15 (American Meteorological Society, 2009).
- Wotton, B. M. Interpreting and using outputs from the Canadian Forest Fire Danger Rating System in research applications. *Environ. Ecol. Stat.* **16**, 107–131 (2009).
- Bistinas, I., Harrison, S., Prentice, I. & Pereira, J. Causal relationships versus emergent patterns in the global controls of fire frequency. *Biogeosciences* **11**, 5087–5101 (2014).
- Viney, N. R. A review of fine fuel moisture modelling. *Int. J. Wildland Fire* **1**, 215–234 (1991).
- Cohen, J. D. & Deeming, J. E. *The National Fire-danger Rating System: Basic Equations* General Technical Report PSW-82 16 (U.S. Department of Agriculture, Forest Service, 1985).
- Schmit, T. J. et al. A closer look at the ABI on the GOES-R series. *Bull. Am. Meteorol. Soc.* **98**, 681–698 (2017).
- Hersbach, H. et al. The ERA5 global reanalysis. *Q. J. R. Meteorol. Soc.* **146**, 1999–2049 (2020).
- Wooster, M. J. et al. Satellite remote sensing of active fires: history and current status, applications and future requirements. *Remote Sens. Environ.* **267**, 112694 (2021).
- Podur, J. & Wotton, B. M. Defining fire spread event days for fire-growth modelling. *Int. J. Wildland Fire* **20**, 497–507 (2011).
- Ho, T. K. in *Proc. 3rd International Conference on Document Analysis and Recognition* 278–282 (IEEE, 1995).
- Zachariassen, J., Zeller, K. F., Nikolov, N. & McClelland, T. A Review of the Forest Service Remote Automated Weather Station (RAWS) Network General Technical Report RMRS-GTR-119 (U.S. Department of Agriculture, Forest Service, 2003).
- Scholten, R. C., Jandt, R., Miller, E. A., Rogers, B. M. & Veraverbeke, S. Overwintering fires in boreal forests. *Nature* **593**, 399–404 (2021).
- Vincent, G. E. et al. Sleep in wildland firefighters: what do we know and why does it matter? *Int. J. Wildland Fire* **27**, 73–84 (2018).
- Page, W. G., Freeborn, P. H., Butler, B. W. & Jolly, W. M. A review of US wildland firefighter entrappings: trends, important environmental factors and research needs. *Int. J. Wildland Fire* **28**, 551–569 (2019).
- Tymstra, C., Stocks, B. J., Cai, X. & Flannigan, M. D. Wildfire management in Canada: review, challenges and opportunities. *Prog. Disaster Sci.* **5**, 100045 (2020).
- Tymstra, C., Jain, P. & Flannigan, M. D. Characterisation of initial fire weather conditions for large spring wildfires in Alberta, Canada. *Int. J. Wildland Fire* **30**, 823–835 (2021).
- van Wageningen, J. W. in *Fire in California's Ecosystems* (eds Sugihara, N. G. et al.) 38–57 (Univ. California Press, 2006).
- Wang, X. et al. Projected changes in fire size from daily spread potential in Canada over the 21st century. *Environ. Res. Lett.* **15**, 104048 (2020).
- Bowman, D. M. et al. Vegetation fires in the Anthropocene. *Nat. Rev. Earth Environ.* **1**, 500–515 (2020).
- Williams, A. P. et al. Observed impacts of anthropogenic climate change on wildfire in California. *Earths Future* **7**, 892–910 (2019).
- Vose, R. S., Easterling, D. R. & Gleason, B. Maximum and minimum temperature trends for the globe: an update through 2004. *Geophys. Res. Lett.* **32**, L23822 (2005).
- Yuan, X. et al. A global transition to flash droughts under climate change. *Science* **380**, 187–191 (2023).
- Flannigan, M. D., Krawchuk, M. A., de Groot, W. J., Wotton, B. M. & Gowman, L. M. Implications of changing climate for global wildland fire. *Int. J. Wildland Fire* **18**, 483–507 (2009).
- Wang, X. et al. Increasing frequency of extreme fire weather in Canada with climate change. *Clim. Change* **130**, 573–586 (2015).

Publisher's note Springer Nature remains neutral with regard to jurisdictional claims in published maps and institutional affiliations.

Springer Nature or its licensor (e.g. a society or other partner) holds exclusive rights to this article under a publishing agreement with the author(s) or other rightsholder(s); author self-archiving of the accepted manuscript version of this article is solely governed by the terms of such publishing agreement and applicable law.

© The Author(s), under exclusive licence to Springer Nature Limited 2024

Methods

Study area and biome categorization

The domain of this study covers the continental United States and Canada. We defined our study area based on the biome categorization from ref. 50 and following the approach of ref. 9, but further combined boreal coniferous forest, boreal mountain system and boreal tundra woodland into an integrated biome 'boreal' for analysis. The resulting 12 classes (Fig. 1) represent biomes with broadly homogeneous climate and vegetation characteristics, specifically, one boreal biome, one tropical biome, five temperate biomes (continental forest, oceanic forest, mountain system (west and east), steppe and desert) and five subtropical biomes (humid forest, dry forest, mountain system, steppe and desert). Given that no OBE was observed in the eastern area of the temperate mountain system biome, all discussion of this biome refers to the areas located in western North America.

Wildland fire geospatial databases

Three wildland fire databases were used in this study: the Canadian National Burned Area Composite (NBAC)⁵¹, the USA Monitoring Trends in Burn Severity (MTBS)⁵² and the Combined Wildland Fire Polygons (CWFP) datasets⁵³. The NBAC is part of the Fire Monitoring, Accounting and Reporting System (FireMARS), jointly developed by the Canada Centre for Mapping and Earth Observation of Natural Resources Canada and the Canadian Forest Service. The NBAC maps the polygon area burned in Canada from 1986 to 2020 (version 20210810) derived from 30-m Landsat imagery and high-quality agency imagery of spatial resolution <30 m. It provides attributes including detected start and end dates, reported start and end dates, fire size and fire cause.

The MTBS is maintained by the U.S. Geological Survey Center for Earth Resources Observation and Science (EROS) and the USDA Forest Service Geospatial Technology and Applications Center (GTAC). It maps burn severity and extent of fires across all lands of the United States from 1984 to 2020 (data released on 28 April 2022). It includes all fires $\geq 1,000$ acres (about 405 ha) in the western United States and ≥ 500 acres (about 202 ha) in the eastern United States and provides attributes such as ignition date and area burned⁵². The CWFP uses a collection of 40 distinct fire layers, using a combination of manual processes and scripts to merge these various datasets into a singular comprehensive dataset. It encompasses recorded information on both wildfires and prescribed fires that have occurred in the United States and specific territories, offering an all-encompassing view of fires that have burned over the past few centuries, spanning from 1835 to 2020. The U.S. Geological Survey released this CWFP dataset on 8 December 2021. For USA fire datasets, we used fires smaller than 405 ha from the CWFP as a complementary dataset to the larger wildfires, exceeding 405 ha, obtained from the MTBS.

Moreover, we used these three fire databases to calculate both the proportion of fires larger than 1,000 ha to the total number of fires and the proportion of their burned area to the total burned area of all fires in the study area.

Geostationary active fire detections

The Fire/Hot Spot Characterization Full Disk (FDCF) products from both GOES-16 (May 2017 to present) and GOES-17 (August 2018 to present) were used to obtain the subhourly active fire detections ('hotspots') in North America during the period 2017–2020. The FDCF products were downloaded from their first available dates to 2020. These products use both visible and infrared Advanced Baseline Imager (ABI) spectral bands to locate fires and retrieve subpixel fire characterizations with 5–15-min temporal resolution and a nominal 2-km spatial resolution (coarser with increasing distance from the subsatellite point)³¹. These satellites are positioned at 75.2° W and 137.2° W, respectively, and can observe the entire burnable land in North and South America when used together. The night-time active fire detection algorithm is considered

to be more sensitive to smaller and/or cooler fires than the daytime algorithm because ambient background temperatures are more homogeneous and lower at night, increasing the potential contrast provided by active fire pixels³³.

Notably, the availability, frequency and quality of the fire detection data varied both regionally and over the course of the study period, as a result of the sequential launch of GOES-16 and GOES-17, changes in imaging frequency and the coverage area and view zenith angle (VZA) of each instrument (see below for more detail on these variations). Owing to these influences, we restrict our use of the hotspot dataset here to identifying the hourly burning status of the individual fires recorded in the wildland fire databases. The available hotspot data had a minimum observation frequency of four times per hour at any location within the study area and, as such, we considered these data fit for this purpose.

Specifically, given the sequential launch and commissioning of GOES-16 and GOES-17 and the different coverage areas of each satellite, data availability is not consistent across North America between 2017 and 2020 (Extended Data Fig. 9a,b). The FDCF of northwestern North America (an area including Alaska and the Yukon) is not imaged by GOES-16 and so hotspot data are only available for this region following the launch of GOES-17 and subsequent FDCF product generation (August 2018 to December 2020). Similarly, northeastern North America is only imaged by GOES-16, so although data are available here for the entire 2017–2020 period, all hotspots identified in this region were solely detected by GOES-16. In central North America, approximately twice as many images, and therefore fire products, were available after the launch of GOES-17 and subsequent FDCF product generation than beforehand, when the only source of GOES-R hotspots for the region was GOES-16.

Moreover, during the 2017–2020 period, the scanning mode of GOES-16 and GOES-17 has changed over time to meet changing operational and experimental needs (Extended Data Fig. 9c,d). Availability of full disk imagery, and the FDCF products derived from it, has therefore varied in frequency between 5 min (Mode 4), 15 min (Mode 3) and 10 min (Mode 6). In 2017 and 2018, Mode 3 was the most common operating mode (that is, 15-min temporal resolution data), whereas in 2019 and 2020, Mode 6 was the dominant operating mode (that is, 10-min data). As a result, more hotspot data are available for the later part of the 2017–2020 period. For more information on GOES scanning mode specifics, see <https://www.goes-r.gov/>.

As the GOES-R satellites are in geostationary orbits, each ground-point location within the study area has a fixed VZA with respect to each GOES instrument. VZA influences the accuracy of fire detection algorithms in several ways^{54,55}. For our study, the fact that the hotspot omission error rate increases with VZA required careful consideration and prevented us from performing detailed direct OBE intercomparisons between biomes with very different VZAs.

Hourly fire diurnal cycle and OBE identification

We developed an algorithm to characterize the hourly fire diurnal cycle of all fires in the NBAC and the combined MTBS–CWFP datasets and identify OBEs. The start (end) date for fires in the NBAC was the earlier (later) date between the detected start (end) date and the reported start (end) date. For fires in the MTBS, the start date was the recorded ignition date. As the MTBS does not contain information on fire end dates, end dates were inferred from the GOES-R hotspot data based on the last date on which two consecutively active burning hours were determined. The same approach was used to infer start and end dates for NBAC and CWFP fires with missing start and end date records. GOES-R hotspots intersecting fire perimeters from the fire start and end dates were extracted.

Fires without matching hotspots from 2017 to 2020 were excluded from further analysis. Fires may be missing corresponding hotspot data owing to active fire detection algorithm omission errors³³, as well as the aforementioned data gaps in the GOES-R active record. We added

a 500-m buffer on the perimeter of fires smaller than 200 ha to reduce the effect of potential geolocation errors on matching up active fire detections with relatively small fires. The resulting hourly fire activity data were converted from Coordinated Universal Time (UTC) time zone to local time zones based on the spatial centroid of the fire perimeters and day of year. The exact times of sunrise and sunset were used to separate daytime and night-time for each day, with sunrise referring to the top edge of the sun appearing on the horizon and sunset referring to the top edge of the sun disappearing below the horizon. Using these local times, each hour was designated as either a daytime or a night-time hour, with night-time hours defined as the first hour after sunset to the last hour before sunrise. Each hour was further assigned to one of four categories: active daytime, non-active daytime, active night-time or non-active night-time. A fire was considered active in a specific hour when at least one hotspot was detected within its perimeter during that hour. For each night when the night-time duration was longer than 4 h and all night-time hours were classified as active, the night was classified as an OBE (that is, a night when a fire burns through the entire night). Nights on which fire activity did not occur in every night-time hour were classified as non-OBEs. The 4-h night-time duration threshold was applied to exclude part of nights of high-latitude summer fires from further analysis. This is because the extent of weather and fine fuel moisture fluctuations is limited during very short night-time periods^{56,57}, making it unsuitable for studying the impact of changes in night-time conditions on overnight burning. Time-zone conversions and local sunrise and sunset times were obtained through the use of R packages *lutz* and *suncalc*.

GOES-R versus low-Earth-orbit satellites active fire detection

To confirm the suitability of using GOES-R to identify OBEs, we examined how frequently fire activity was observed by three independent low-Earth-orbit satellite systems when they provided imagery temporally and spatially coincident with OBEs: Suomi National Polar-orbiting Partnership (NPP) with Visible Infrared Imaging Radiometer Suite (VIIRS)⁵⁸ and Terra and Aqua with Moderate Resolution Imaging Spectroradiometer (MODIS)⁵⁹. For each OBE, we examined the number of corresponding overpasses and the fire activity per overpass within the fire perimeter at the time of OBE occurrence. We used the MODIS GeoMeta Collection 6.1 and geoMetaVIIRS products to reconstruct historic overpass information and used MODIS and VIIRS hotspot information from the NASA Fire Information for Resource Management System.

We found that 98.3% (1,694/1,724) of Suomi NPP, 95.5% (1,284/1,344) of Terra and 91.6% (1,206/1,317) of Aqua overpasses coincident with OBEs had associated active fire observations, supporting our use of GOES-R for OBE identification. Notably, Suomi NPP, Terra and Aqua provided on average just 1.57, 1.23 and 1.20 observations per OBE, respectively, despite the average night-time duration of OBEs being 10.13 h.

Fire weather calculation and extraction

In this study, meteorological variables provided by ERA5 reanalysis data were used to process and calculate fire weather from 1979 to 2020, including the inputs and components of the CFWIS as well as VPD. ERA5 is the fifth generation of global hourly atmospheric reanalysis produced by the European Centre for Medium-Range Weather Forecasts (ECMWF) and is widely used in wildfire studies⁶⁰. It resolves the atmosphere using 137 levels from the surface up to a height of 80 km on a 31-km horizontal grid⁹.

The CFWIS usually outputs six daily components by first tracking moisture in three fuel layers of varying depth with corresponding moisture codes: Fine Fuel Moisture Code (FFMC, litter and fine fuels), Duff Moisture Code (DMC, organic fuels at moderate depth) and Drought Code (DC, deep and compact organic fuels). The remaining three components are potential fire behaviour indices: Initial Spread Index (ISI, the rate of fire spread), Buildup Index (BUI, the cumulative fuel

availability) and Fire Weather Index (FWI, the fire intensity). To account for the impact of diurnal fluctuations in weather and surface fine fuel moisture on OBEs, the hourly FFMC and ISI were calculated using the procedures outlined in refs. 57,61. The hourly FFMC calculation was based on the hourly weather observations of 2-m temperature (T , °C), relative humidity (RH), wind speed (WS, km h^{-1}) and precipitation, as well as the previous hour's weather conditions. RH was calculated from 2-m T and 2-m dew point T following equations (1) and (2) in ref. 62. WS was calculated from 10-m U (zonal velocity) and V (meridional velocity). The hourly ISI combined hourly FFMC and hourly WS. The hourly VPD (kPa) was calculated on the basis of the conversion equation from ref. 63 using 2-m T and 2-m dew point T . The remaining four components of the CFWIS (FWI, DMC, DC and BUI) were obtained from ref. 9 at daily temporal resolution, as they or their subcomponents are slow-reacting to weather fluctuations. We extracted the aforementioned fire weather variables for each fire during its lifetime, buffering 24 h at the start date, and then time-matched these data with the corresponding fire diurnal cycles. For each time step, data were spatially averaged across all grid cells intersected by a given fire perimeter.

The spatiotemporal distribution and statistics of OBEs

We summarized the spatial and temporal distribution of OBEs by biome and season. OBE fires were further categorized into single-OBE fires and multi-OBE fires, in which only one OBE and more than one OBE occurred, respectively. The proportion of multi-OBE fires to all OBE fires and the mean number of OBEs per multi-OBE fire was calculated by biome.

Extreme characteristics of OBEs

We summarized the number of OBEs and OBE fires in seven fire-size categories: 0–200 ha, 200–1,000 ha, 1,000–10,000 ha, 10,000–20,000 ha, 20,000–50,000 ha, 50,000–100,000 ha and >100,000 ha. Linear regression (significance level: 0.05) was used to investigate the relationship between the number of OBEs and fire size for OBE fires in all biomes, as well as separately in boreal, temperate mountain system and subtropical mountain system (three main biomes with the most OBEs). Moreover, we calculated the number of days between ignition and the occurrence of the first OBE in each OBE fire and the number of days between two adjacent OBEs in each multi-OBE fire to evaluate the succession of OBEs and the potential impact of OBEs on fire management.

Comparison of fire weather conditions

Given that 99% of OBEs were detected in fires larger than 1,000 ha, we focused our analysis on these large fires to investigate the underlying factors contributing to OBEs. We examined the differences in the fire weather between OBEs and non-OBEs (including non-OBEs during OBE fires) within fires larger than 1,000 ha in the five main biome–season groups with 100 or more OBEs (boreal summer, temperate mountain system summer and autumn and subtropical mountain system summer and autumn) using a one-sided Mann–Whitney U test (significance level: 0.05) to investigate significant drivers of OBEs. Mann–Whitney U test was selected because the distribution of some variables was skewed. Using the same test, we also evaluated differences in the day–night range of hourly variables between OBEs and non-OBEs, as we suggested that a smaller diurnal range in fire weather may facilitate the occurrence of an OBE. These ranges were $\text{FFMC}_{\text{Dmax-Nmin}}$, $\text{ISI}_{\text{Dmax-Nmin}}$, $\text{RH}_{\text{Dmin-Nmax}}$, $\text{T}_{\text{Dmax-Nmin}}$ and $\text{VPD}_{\text{Dmax-Nmin}}$.

Assessment of an increasing trend in OBE fire weather extremes

To assess the fire weather extremes for OBEs, we calculated the percentile value of each OBE's fire weather variable from fires larger than 1,000 ha relative to the distribution of values extracted from records for the years 2000–2020 and 1979–1999 in the corresponding fire perimeter. The fire weather variables examined were the four daily

Article

components (FWI, BUI, DMC and DC) of the CFWIS and, based on hourly variables, the daytime extrema (FFMC_{Dmax}, ISI_{Dmax}, VPD_{Dmax}, T_{Dmax} and RH_{Dmin}) and night-time extrema (FFMC_{Nmin}, ISI_{Nmin}, VPD_{Nmin}, T_{Nmin} and RH_{Nmax}), capturing the changes of slow-reacting and fast-reacting fuel and weather dynamics. We then used a paired Wilcoxon test to compare these two percentiles for each OBE's fire weather variable to determine whether there has been a change in fire weather between the two time periods.

Importance analysis of fire weather variables

We aimed to understand the dominant factors influencing OBEs by building random forest models³⁵ to analyse the relationship between fire weather and OBE occurrence within fires larger than 1,000 ha in the five main biome–season groups (see 'Comparison of fire weather conditions'). The random forest models were built using a binary dependent variable (OBE or non-OBE) and all fire weather variables as the explanatory variables, except the ranges of fast-reacting variables, most of which showed no significant differences between OBEs and non-OBEs. Random forest is an ensemble approach that consists of many individual decision trees, which take input from randomly bootstrapped variables and samples. In random forest ensembles, we chose 500 trees in each forest and a depth of 1 for each tree. By setting the tree depth to 1, both hierarchical relationships and interactions between variables would be avoided. To ensure statistically reliable results, we repeated the process 50 times using fivefold cross-validation. To resolve the impact of the disparity in frequencies of the two classes, non-OBEs data were downsampled in each training. We used the mean decrease in the Gini coefficient (that is, Gini importance) to measure how each variable contributes to the impurity decreases of the tree nodes in the resulting random forest. The higher the value of the Gini importance, the higher the importance of the variable in the model. We normalized the Gini importance values and used the area under receiver operator characterization (ROC) curve (AUC)⁶⁴ to evaluate the performance of models. Model construction and performance evaluation were performed using the R package caret⁶⁵.

Simply adding all OBEs and non-OBEs from fires <1,000 ha into the variable importance analysis would be problematic, as it would lead to the inclusion of many non-OBEs from fires without OBEs into the dataset. This would considerably skew the proportion of OBEs to non-OBEs and OBEs would primarily be associated with large fires, whereas non-OBEs would primarily be associated with small fires. To avoid this issue, we conducted a further analysis similar to the above-mentioned random-forest-based variable importance analysis but adopting a stratified sampling approach to include all OBEs and an equivalent number of non-OBEs for each biome–season group in each fire-size category: 0–200 ha, 200–1,000 ha, 1,000–10,000 ha, 10,000–20,000 ha, 20,000–50,000 ha, 50,000–100,000 ha and >100,000 ha. We repeated this stratified sampling ten times and, for each stratified sampling, we performed a 50 times fivefold cross-validation, then averaged the results to ensure the robustness of this analysis.

Two large-fire case studies were selected to demonstrate the relation between the occurrence and consecutive occurrence of OBEs and fire weather varying in time and space: the 2020 Creek Fire (California, subtropical mountain system) and the 2019 McMillan Complex wildfire (Alberta, boreal).

Prediction of OBEs

To explore the potential predictability of OBEs (that is, whether the coming night is an OBE or not) and to understand the coupling between daytime conditions and night-time burning, we constructed logistic regression models for nights of fires larger than 1,000 ha in five main biome–season groups (see 'Comparison of fire weather conditions') using either a single daily variable (four models) or a combination of several daily variables (11 models). We discarded models that incorporated several variables if the variance inflation factor of any variable

was greater than 2 to avoid multicollinearity. Similarly, 50 times fivefold cross-validation and downsampling in each training were also performed for each prediction model. Model performance was evaluated using ROC, AUC, recall (that is, the proportion of OBEs that were successfully predicted by the model) and false positive rate. The best models were determined by both AUC (primary criterion) and recall (secondary criterion). Model building and performance evaluation were conducted using the R package caret.

Data availability

The datasets for conducting the analysis presented here are all publicly available. The NBAC, MTBS and CFWP wildland fire datasets are respectively available from the Canadian Forest Service (<https://cwfis.cfs.nrcan.gc.ca/datamart/metadata/nbac>), <https://www.mtbs.gov/> and the U.S. Geological Survey (<https://data.usgs.gov/datacatalog/data/USGS:61707c2ad34ea36449a6b066>). The GOES-16 and GOES-17 full disk active fire products are available on Amazon Web Service S3 Explorer (<https://registry.opendata.aws/noaa-goes/>). The hourly ERA5 climate data used for this study are available at <https://doi.org/10.24381/cds.adbb2d47>. The biome categorizations used in this study are available at <https://www.worldwildlife.org/publications/terrestrial-ecoregions-of-the-world>. The MODIS GeoMeta Collection 6.1 and geoMetaVIIRS products for reconstructing overpasses are from the Level-1 and Atmosphere Archive & Distribution System (<https://ladsweb.modaps.eosdis.nasa.gov/archive>). The MODIS and VIIRS active fire products were obtained from the Fire Information for Resource Management System (<https://firms.modaps.eosdis.nasa.gov/download/>). Source data are provided with this paper.

Code availability

Codes used to analyse the data are available from <https://github.com/KaiweiLL/overnight-fires> or <https://doi.org/10.5281/zenodo.10278113>.

- Olson, D. M. et al. Terrestrial ecoregions of the world: a new map of life on Earth: a new global map of terrestrial ecoregions provides an innovative tool for conserving biodiversity. *BioScience* **51**, 933–938 (2001).
- Hall, R. et al. Generating annual estimates of forest fire disturbance in Canada: the National Burned Area Composite. *Int. J. Wildland Fire* **29**, 878–891 (2020).
- Eidenshink, J. et al. A project for monitoring trends in burn severity. *Fire Ecol.* **3**, 3–21 (2007).
- Welty, J. & Jeffries, M. *Combined Wildland Fire Datasets for the United States and Certain Territories, 1800s-Present* (U.S. Geological Survey, 2021); <https://doi.org/10.5066/P9ZXFY3>.
- Hall, J. V., Zhang, R., Schroeder, W., Huang, C. & Giglio, L. Validation of GOES-16 ABI and MSG SEVIRI active fire products. *Int. J. Appl. Earth Obs. Geoinf.* **83**, 101928 (2019).
- Wooster, M. J. et al. Meteosat SEVIRI Fire Radiative Power (FRP) products from the Land Surface Analysis Satellite Applications Facility (LSA SAF) – part 1: algorithms, product contents and analysis. *Atmos. Chem. Phys. Discuss.* **15**, 15831–15907 (2015).
- Page, W. G., Jenkins, M. J. & Alexander, M. E. Foliar moisture content variations in lodgepole pine over the diurnal cycle during the red stage of mountain pine beetle attack. *Environ. Model. Softw.* **49**, 98–102 (2013).
- Van Wagner, C. E. *A Method of Computing Fine Fuel Moisture Content Throughout the Diurnal Cycle* Information Report PS-X-69 (Canadian Forestry Service, 1977).
- Schroeder, W., Oliva, P., Giglio, L. & Csizsar, I. A. The New VIIRS 375 m active fire detection data product: algorithm description and initial assessment. *Remote Sens. Environ.* **143**, 85–96 (2014).
- Giglio, L., Schroeder, W. & Justice, C. O. The collection 6 MODIS active fire detection algorithm and fire products. *Remote Sens. Environ.* **178**, 31–41 (2016).
- Di Giuseppe, F. et al. Fire Weather Index: the skill provided by the European Centre for Medium-Range Weather Forecasts ensemble prediction system. *Nat. Hazards Earth Syst. Sci.* **20**, 2365–2378 (2020).
- Wang, X. et al. cffdrs: an R package for the Canadian Forest Fire Danger Rating System. *Ecol. Process.* **6**, 5 (2017).
- McElhinny, M., Beckers, J. F., Hanes, C., Flannigan, M. & Jain, P. A high-resolution reanalysis of global fire weather from 1979 to 2018—overwintering the Drought Code. *Earth Syst. Sci. Data* **12**, 1823–1833 (2020).
- Alduchov, O. A. & Eskridge, R. E. Improved Magnus form approximation of saturation vapor pressure. *J. Appl. Meteorol. Climatol.* **35**, 601–609 (1996).
- Hanley, J. A. & McNeil, B. J. The meaning and use of the area under a receiver operating characteristic (ROC) curve. *Radiology* **143**, 29–36 (1982).
- Kuhn, M. Caret: classification and regression training. Astrophysics Source Code Library, record ascl:1505.003; <https://ascl.net/1505.003> (accessed 20 May 2022).

Acknowledgements This study is supported by Canada Wildfire. K.L. is supported by the China Scholarship Council (202006070013). We thank P. Jain and D. Castellanos-Acuna for providing the fire weather data and C. Guo, S. C. P. Coogan, B. M. Wotton and H. Qian for their suggestions and help.

Author contributions Conceptualization: M.F., X.W. and K.L. Methodology: K.L., X.W., M.F. and M.d.J. Investigation: K.L., X.W., M.F. and M.d.J. Visualization: K.L., X.W. and M.d.J. Funding acquisition: M.F., X.W. and K.L. Project administration: M.F. and X.W. Supervision: M.F. and X.W. Writing—original draft: K.L. and X.W. Writing—review and editing: K.L., X.W., M.d.J. and M.F.

Competing interests The authors declare no competing interests.

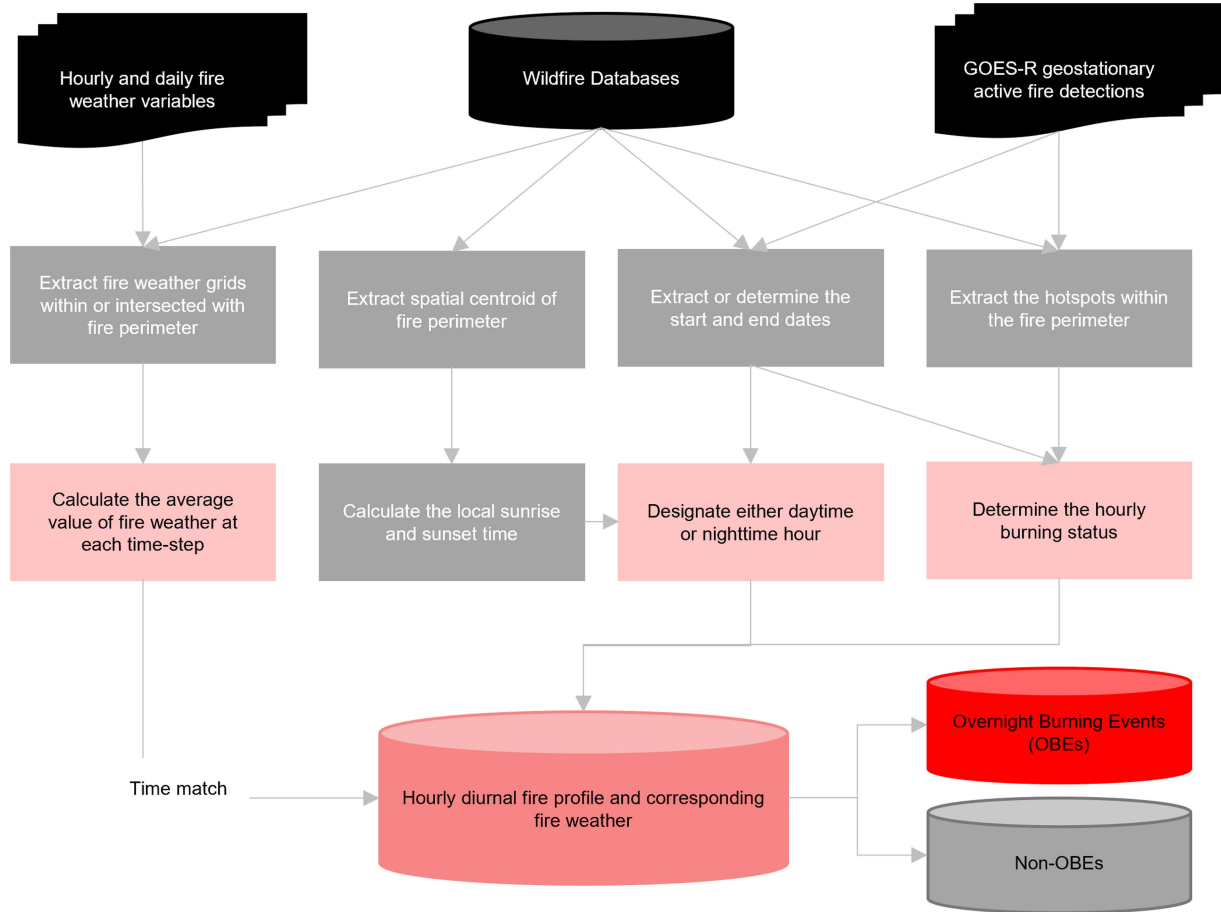
Additional information

Supplementary information The online version contains supplementary material available at <https://doi.org/10.1038/s41586-024-07028-5>.

Correspondence and requests for materials should be addressed to Kaiwei Luo or Xianli Wang.

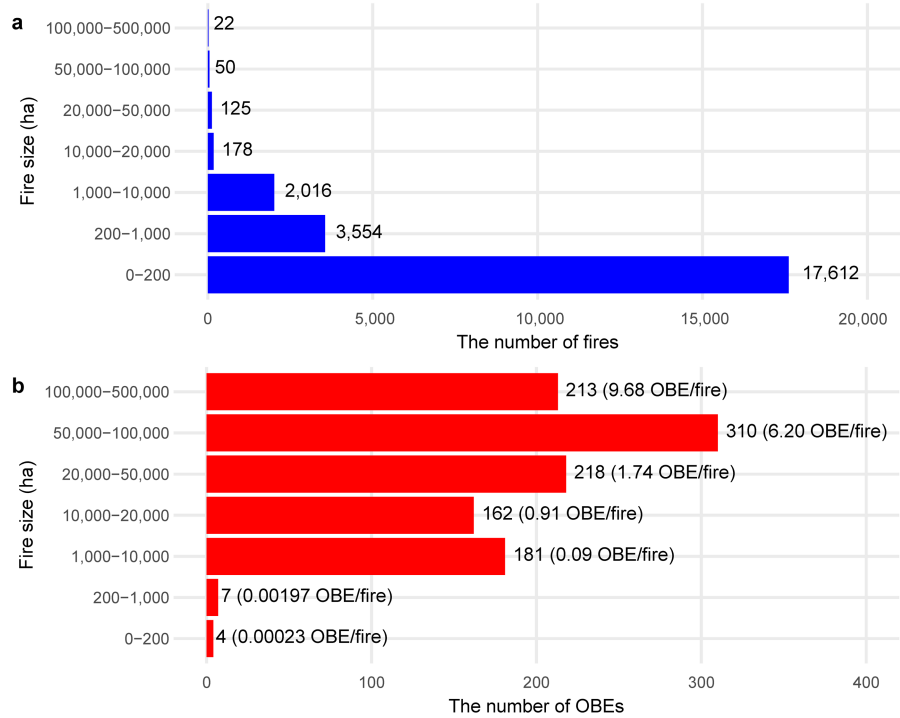
Peer review information *Nature* thanks the anonymous reviewers for their contribution to the peer review of this work. Peer reviewer reports are available.

Reprints and permissions information is available at <http://www.nature.com/reprints>.



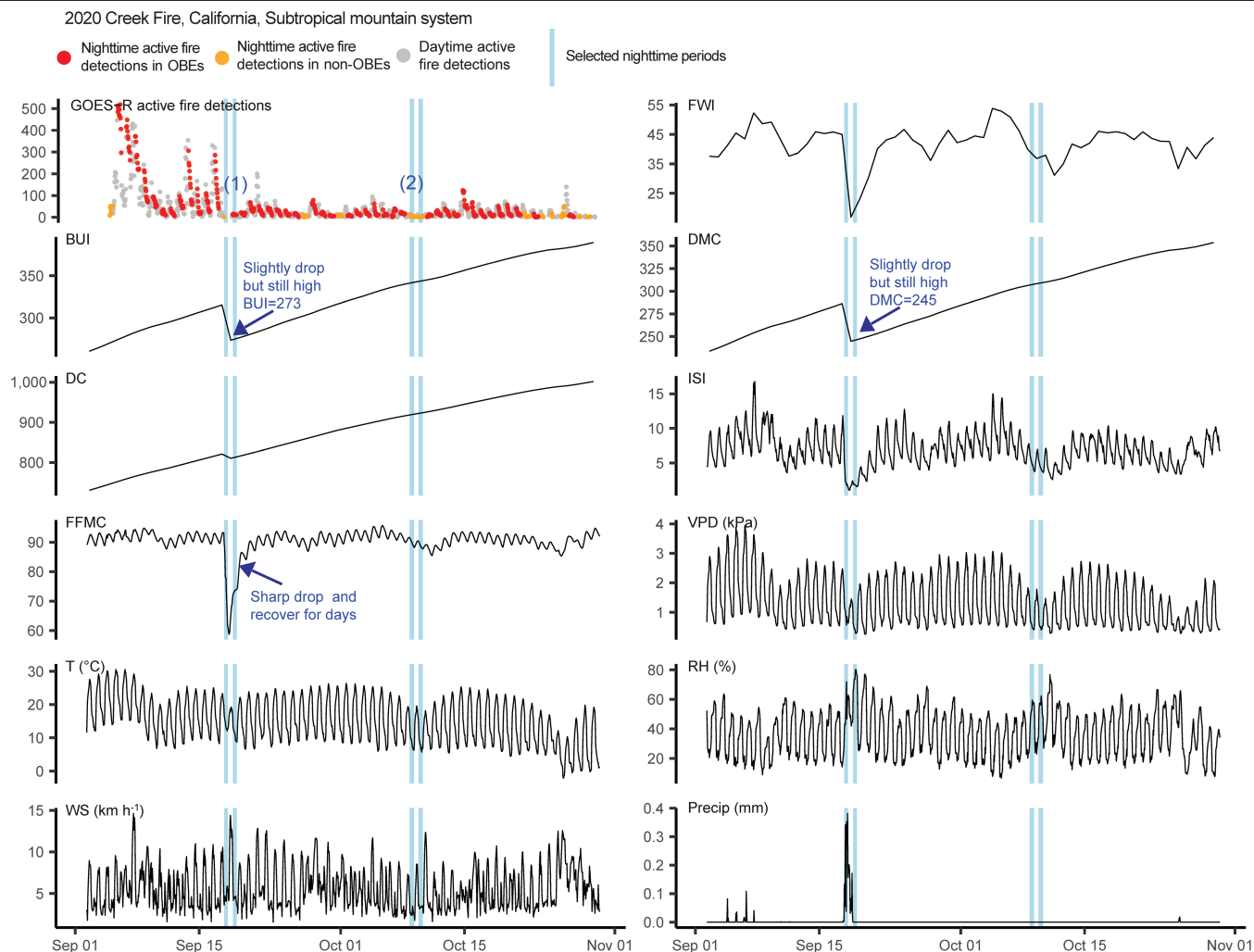
Extended Data Fig. 1 | Data processing workflow used for identifying OBEs and extracting coincident fire weather data. First, the hourly diurnal cycle of each fire was examined using terrestrial wildfire databases and GOES-R active fire detections. Specifically, the hourly burning status of each fire was determined by the combination of the extracted or determined start and end dates and the extracted hotspots within its fire perimeter. Based on the spatial

centroid of the fire perimeter, every hour during each fire’s lifetime was then designated either a daytime or night-time hour. Nights on which fire activity did and did not occur in every night-time hour were classified as OBEs and non-OBEs, respectively. Second, the hourly and daily fire weather grids within or intersected by each fire perimeter were extracted and then time-matched with the hourly diurnal cycle.



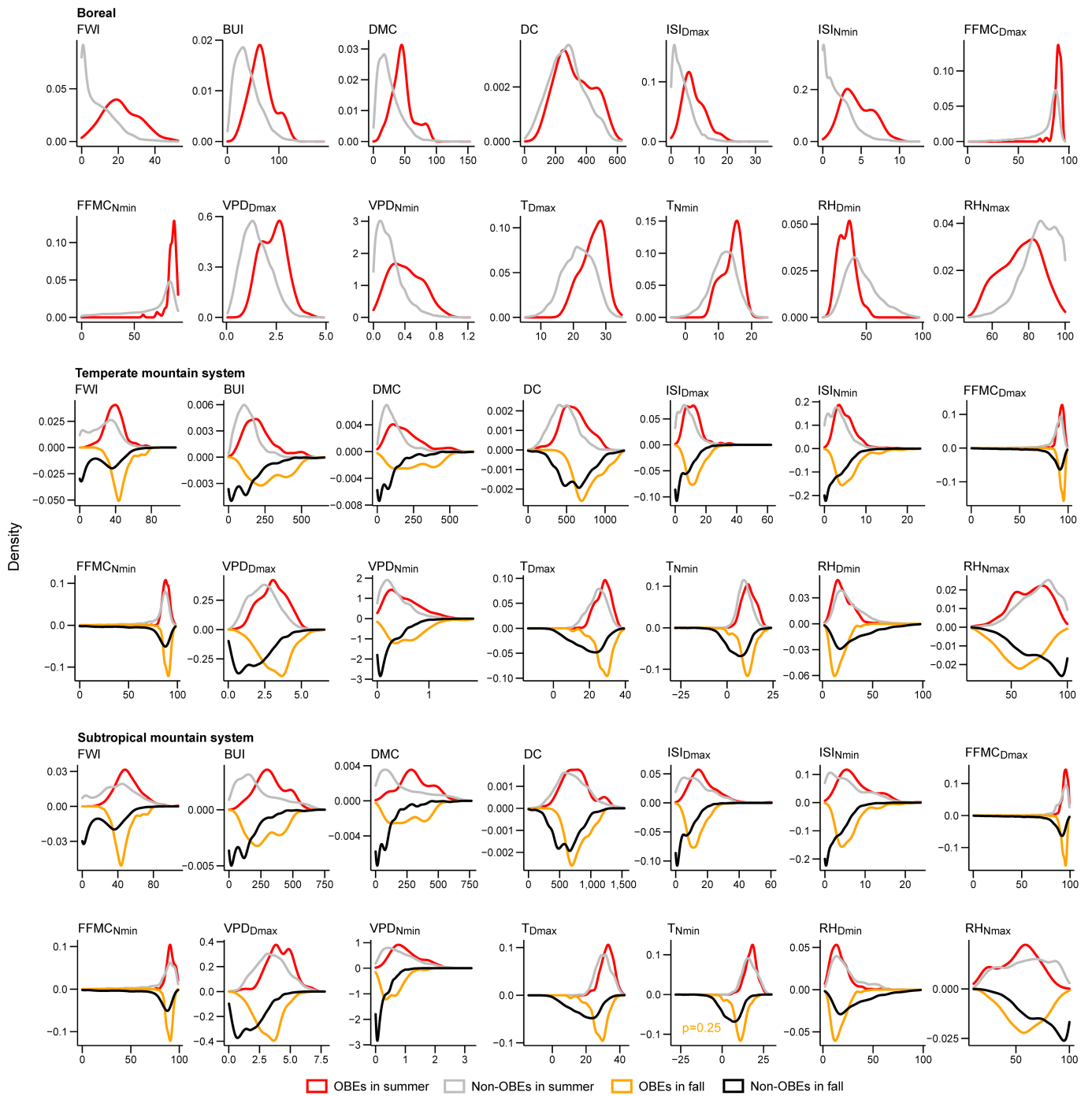
Extended Data Fig. 2 | The number of fires and OBEs categorized by fire size. The number of fires (a) and OBEs (b) categorized by fire size: 0–200 ha, 200–1,000 ha, 1,000–10,000 ha, 10,000–20,000 ha, 20,000–50,000 ha,

50,000–100,000 ha and >100,000 ha in North America during 2017–2020. Furthermore, we computed the ratio between the number of OBEs and the total number of fires in each respective category.



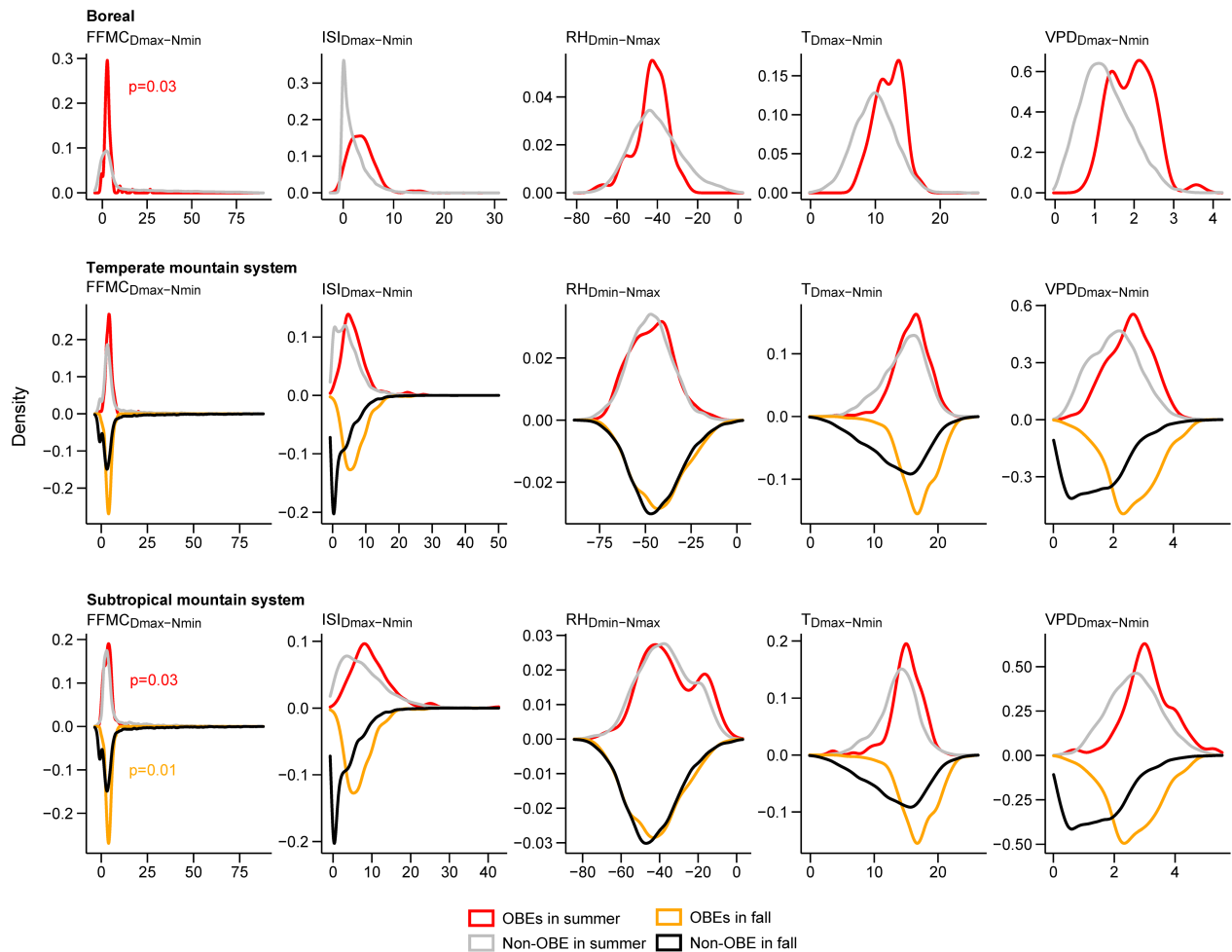
Extended Data Fig. 3 | Active fire detections and coincident fire weather for the 2020 Creek Fire in California, in the subtropical mountain system biome. The top-left plot shows the time series of GOES-R active fire detection hotspots. Hotspots are categorized and coloured according to daytime (grey) and night time (red and orange for night-time hotspots in OBEs and non-OBEs, respectively). The remaining plots show the corresponding fire weather variables as time series. The Creek Fire burned a total of 154,364 ha, with 43 OBEs observed over 52 days from 6 September to 27 October. Despite rainfall

(3.6 mm in total) temporarily putting a stop to OBEs and decreasing fire weather codes and indices on 18 September (see (1)), OBEs quickly resumed on 19 September owing to the dryness of moderately slow-drying fuels (DMC) and high fuel availability (BUI), highlighting the critical role of drought in facilitating overnight burning. However, non-OBEs can still occur when DMC and BUI were high and unaffected (see (2)). These non-OBEs are associated with periods of corresponding changes in the fast-reacting variables adverse to fire spread, such as relatively low temperature and increased RH.



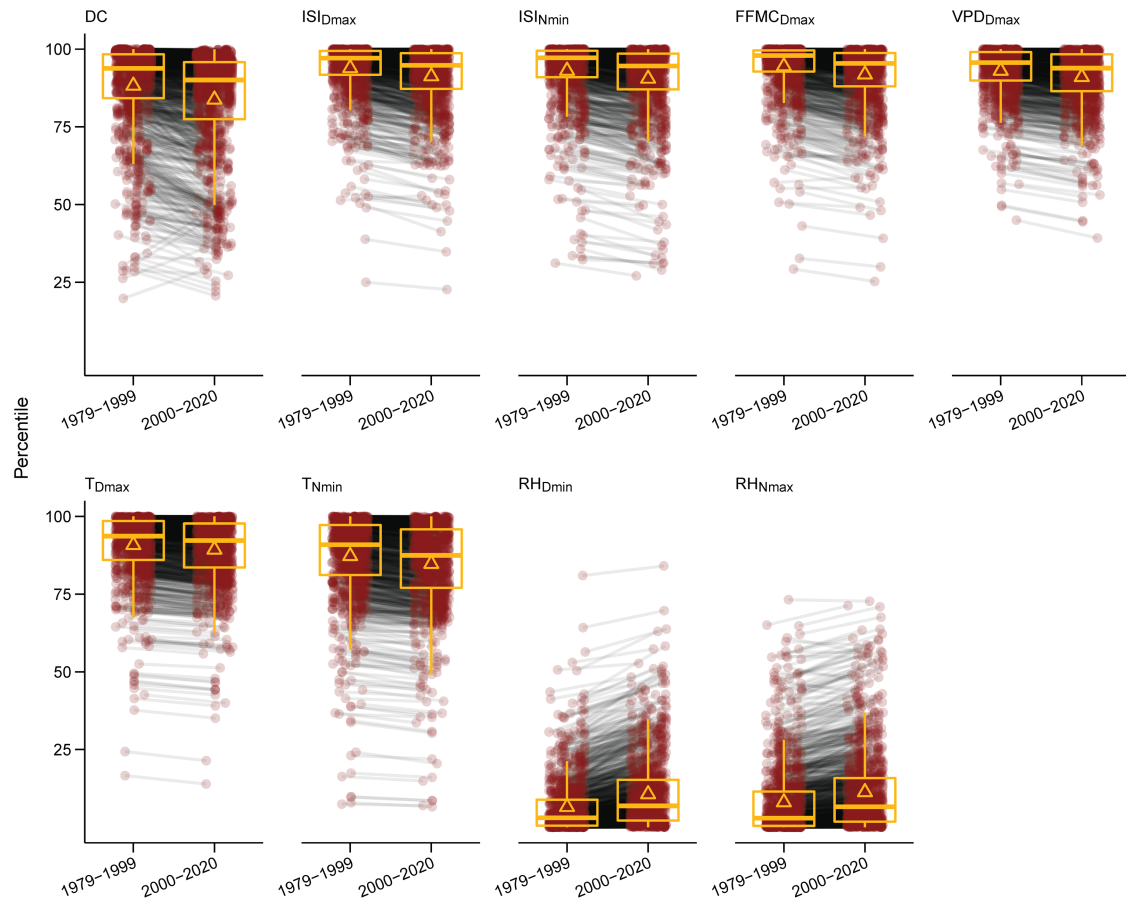
Extended Data Fig. 4 | Comparison of all fire weather variables between OBEs and non-OBEs. Comparison of fire weather conditions during OBEs and non-OBEs within fires larger than 1,000 ha in the boreal, temperate mountain system and subtropical mountain system. For each biome, curves show the density distribution of daily variables and daytime and night-time extrema of hourly variables for OBEs (red for summer and orange for fall) and non-OBEs

(grey for summer and black for fall). We invert the y-axis of the distribution of fire weather variables in fall for better visualization. All variables for OBEs in each biome-season group were significantly greater (or smaller in the case of RH; one-sided Mann-Whitney U test, $P < 0.05$) than those for non-OBEs, except T_{Nmin} in subtropical mountain system fall ($P = 0.25$).



Extended Data Fig. 5 | Comparison of day-night range of hourly fire weather variables between OBEs and non-OBEs. Comparison of day-night range of hourly fire weather variables (FFMC, ISI, RH, T and VPD) between OBEs and non-OBEs within fires larger than 1,000 ha in boreal, temperate mountain system and subtropical mountain system. For each biome, curves show the density distribution of day-night ranges for OBEs (red for summer and orange

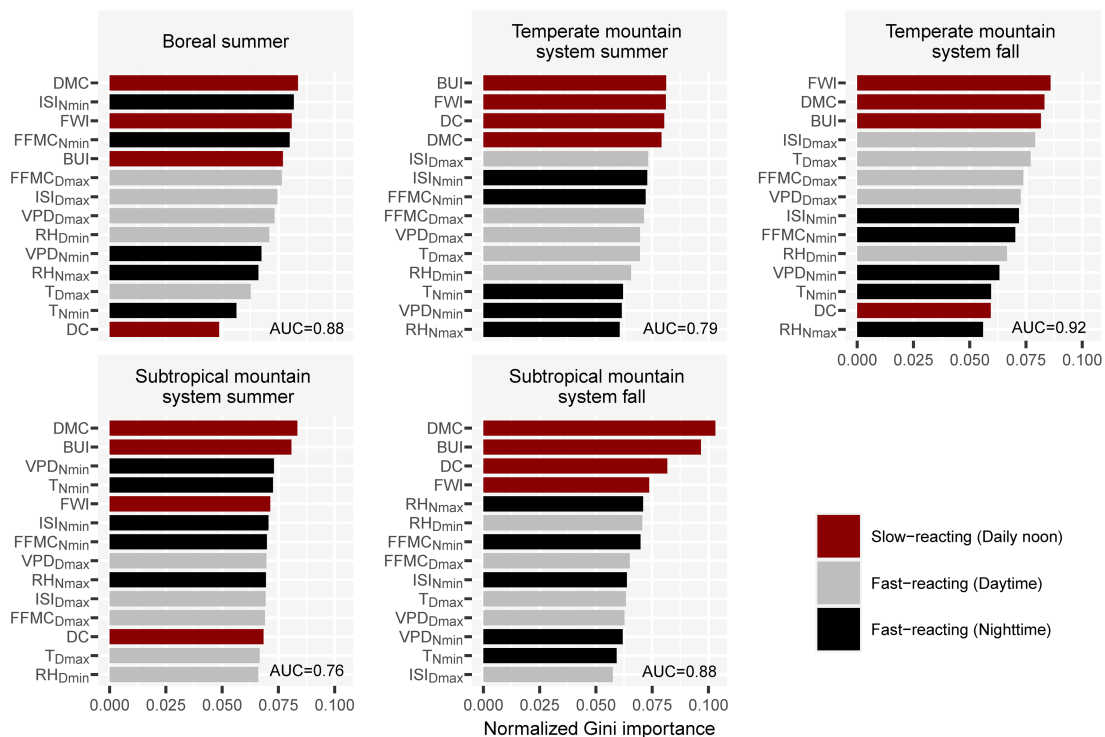
for fall) and non-OBEs (grey for summer and black for fall). We invert the y-axis of the distribution of fire weather variables in fall for better visualization. Only FFMC of OBEs showed a significantly smaller range than non-OBEs (one-sided Mann-Whitney *U* test, $P < 0.05$) in boreal summer ($P = 0.03$) and subtropical mountain system summer ($P = 0.03$) and fall ($P = 0.01$).



Extended Data Fig. 6 | Percentile distributions and statistical significance of selected fire weather variables for OBEs (1979-1999 versus 2000-2020).

The line-linked paired points respectively represent the percentile of fire weather (DC and daytime and/or night-time extrema of ISI, FFMC, VPD, T and RH) for each OBE within fires larger than 1,000 ha relative to comparable observations during the 1979-1999 and 2000-2020 periods at the same geographic location. The 1979-1999 percentiles are significantly higher than

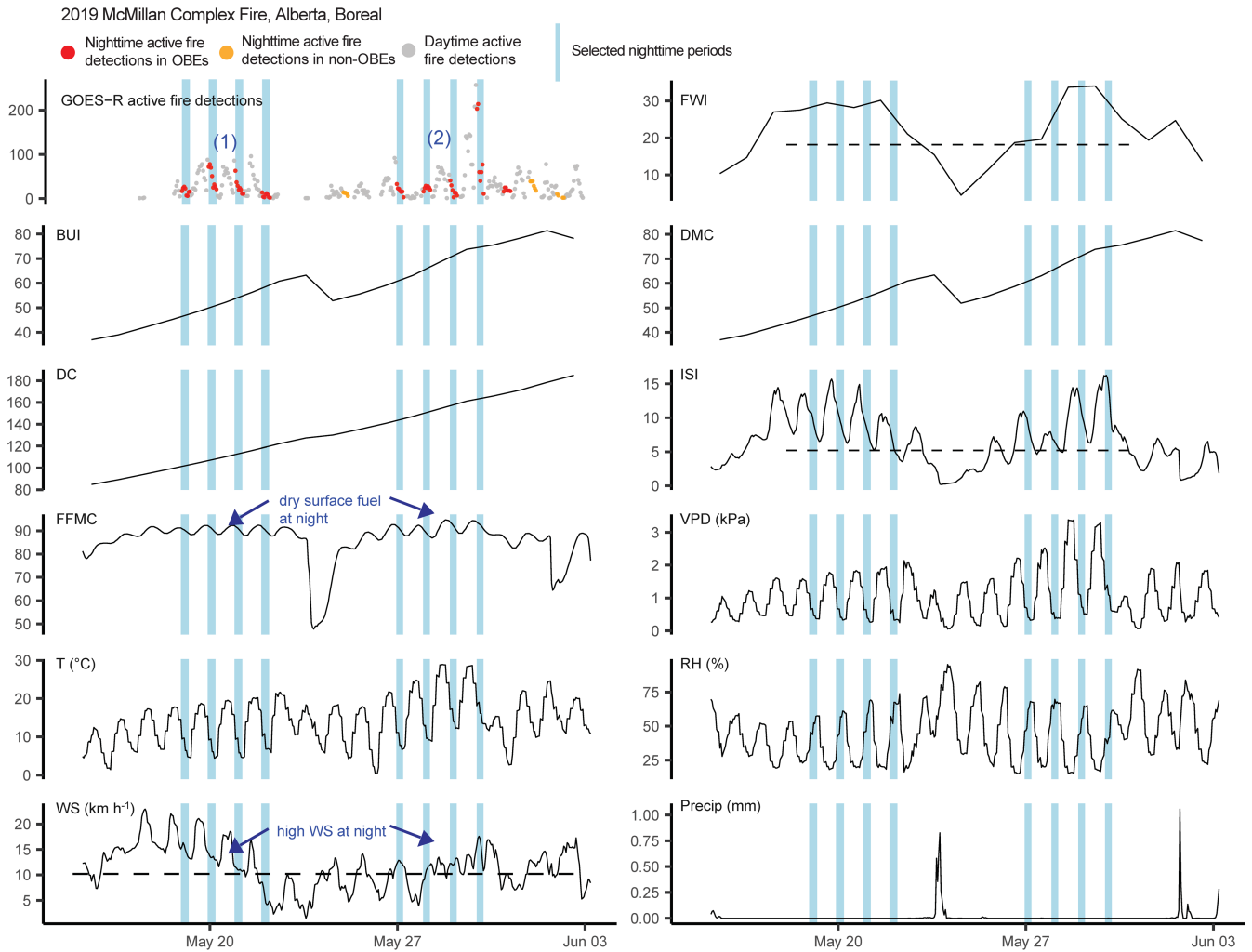
the 2000-2020 percentiles for each fire weather variable (paired Wilcoxon test, $P < 0.05$). Box plots represent the distribution of these percentile values. Each box plot includes a horizontal line to represent the median, a triangle to represent the mean, a box with lower and upper ends that represent the first and third quartiles and whiskers extending from the corresponding ends of the box to the smallest value at most 1.5 times the interquartile range and largest value no further than 1.5 times the interquartile range.



Extended Data Fig. 7 | Fire weather variable importance for OBEs based on random forest modelling and stratified sampling in fire-size categories.

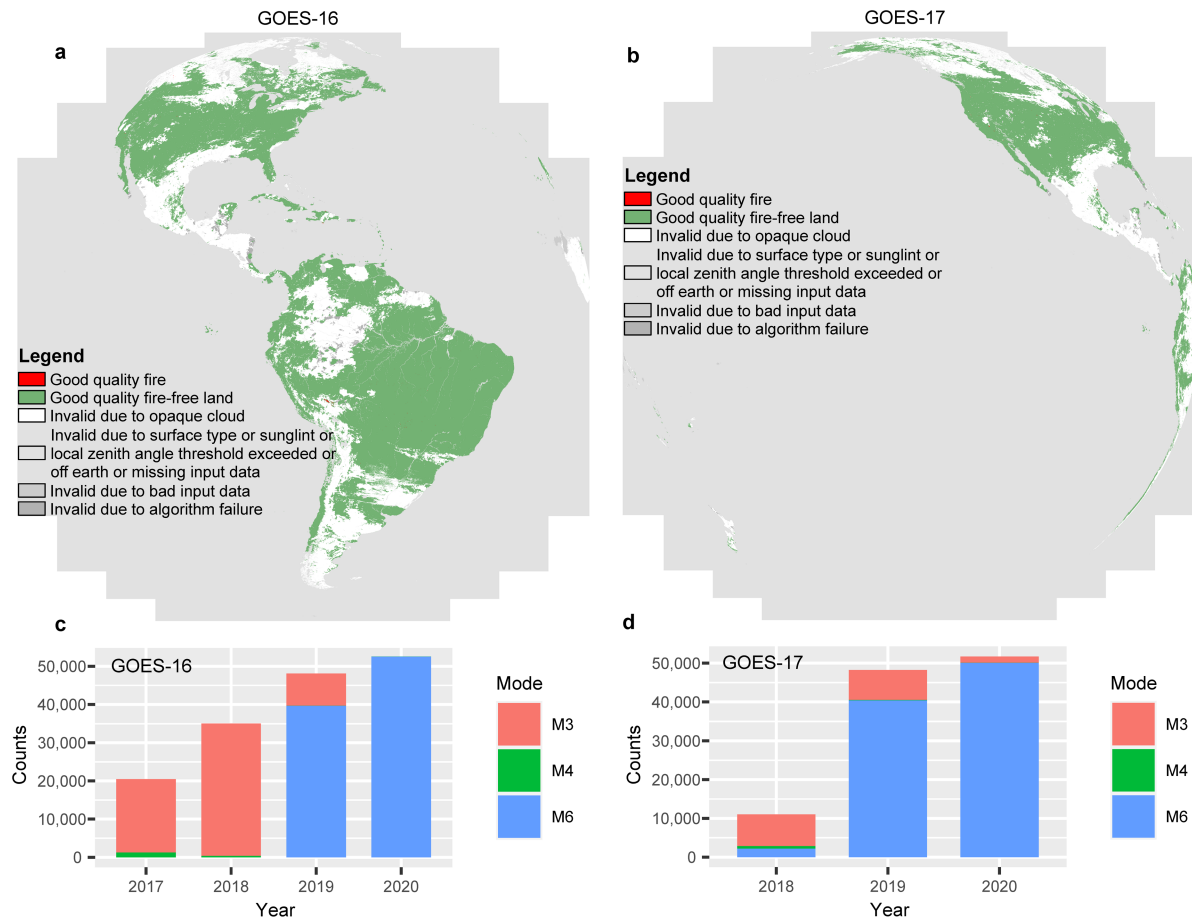
For each main biome–season group, we calculated the normalized mean decreases in the Gini coefficient of fire weather variables. This was done using a random forest model to classify OBEs and non-OBEs. We used a stratified sampling approach that ensured the inclusion of all OBEs, along with an equivalent number of non-OBEs in each biome–season group in each fire-size

category: 0–200 ha, 200–1,000 ha, 1,000–10,000 ha, 10,000–20,000 ha, 20,000–50,000 ha, 50,000–100,000 ha and >100,000 ha. The variables are ranked from the most important to the least important. Slow-reacting variables are represented by dark red horizontal bars and daytime and night-time extrema of fast-reacting variables by grey and black bars, respectively. The performance of the models is evaluated by the area under the receiver operating characteristic curve (AUC).



Extended Data Fig. 8 | Active fire detections and coincident fire weather for the 2019 McMillan Complex wildfire in Alberta, in the boreal biome. The top-left plot shows the time series of GOES-R active fire detection hotspots. Hotspots are categorized and coloured according to daytime (grey) and night time (red and orange for night-time hotspots in OBEs and non-OBEs, respectively). The remaining plots show the corresponding fire weather variables as time series. The McMillan Complex wildfire burned a total of

199,888 ha, with nine OBEs within 13 days from 19 May to 31 May. Two OBEs clusters occurred during the McMillan Complex wildfire centred on 20 May (see (1)) and 29 May (see (2)). During both of these periods, DMC and BUI remained relatively low (although both were 40+). However, high wind speeds and dry surface fine fuel (FFMC) at night time increased fire spread potential (ISI) and fire intensity potential (FWI), thereby facilitating the occurrence of OBEs.



Extended Data Fig. 9 | Coverage and data availability of the GOES-R FDCF products. Data quality flag layers for GOES-16 (image: 2020250020019200000) (a) and GOES-17 (image: 2020250020031900000) (b) illustrate the spatial extent of the FDCF of GOES-R satellite. GOES-16 does not capture the northwestern

area of North America and GOES-17 does not capture the northeastern area of North America. c,d, Number of FDCF products analysed in this study for GOES-16 and GOES-17, respectively, classified by scanning mode.

Extended Data Table 1 | Summary of the total number of OBEs and OBE fires

Biome	OBE fires	Total OBEs	OBEs by seasons				OBEs by fire classes		Persistence
			Spring	Summer	Fall	Winter	Single	Multiple	
Boreal	65	147	36	103	8	0	35	112	3.7
Temperate mountain system	130	492	1	273	218	0	48	444	5.4
Subtropical mountain system	78	335	8	157	169	1	30	305	6.4
Temperate desert	47	77	0	64	13	0	34	43	3.3
Temperate continental forest	2	4	0	4	0	0	1	3	3
Temperate steppe	6	9	3	5	1	0	4	5	2.5
Subtropical desert	6	22	3	18	1	0	3	19	6.3
Subtropical dry forest	0	0	0	0	0	0	0	0	0
Subtropical humid forest	0	0	0	0	0	0	0	0	0
Subtropical steppe	4	6	4	2	0	0	3	3	3
Tropical moist forest	2	3	3	0	0	0	1	2	2
North America	340	1095	58	626	410	1	159	936	5.2

The 'Single' and 'Multiple' columns respectively present the number of OBEs from single-OBE fires and multi-OBE fires. The 'Persistence' column presents the mean number of OBEs for multi-OBE fires. No OBEs were observed in the temperate oceanic forest biome. Season classifications are as follows: spring (March–May); summer (June–August); fall (September–November); winter (December–February).

Article

Extended Data Table 2 | The metrics for prediction models by variable combination and biome–season group

Combination of variables	Boreal			Temperate mountain system						Subtropical mountain system					
	Summer			Summer			Fall			Summer			Fall		
	AUC	Recall	FPR	AUC	Recall	FPR	AUC	Recall	FPR	AUC	Recall	FPR	AUC	Recall	FPR
BUI	0.81	0.74	0.25	0.75	0.63	0.27	0.84	0.73	0.22	0.71	0.64	0.32	0.71	0.79	0.30
DMC	0.82	0.75	0.24	0.75	0.59	0.25	0.84	0.69	0.18	0.72	0.66	0.31	0.72	0.79	0.29
DC	0.61	0.50	0.40	0.72	0.63	0.34	0.74	0.63	0.33	0.57	0.52	0.43	0.60	0.54	0.42
FWI	0.84	0.73	0.24	0.73	0.72	0.38	0.85	0.86	0.28	0.67	0.65	0.39	0.73	0.75	0.37
FWI+BUI	0.84	0.76	0.24	0.77	0.70	0.32	0.87	0.83	0.26	0.70	0.71	0.38	0.72	0.78	0.38
FWI+DMC	0.84	0.77	0.23	0.77	0.69	0.33	0.87	0.82	0.26	0.71	0.72	0.37	0.73	0.78	0.37
FWI+DC	0.83	0.73	0.24	0.76	0.73	0.34	0.85	0.84	0.28	0.67	0.67	0.43	0.73	0.75	0.37
DMC+DC	0.83	0.77	0.24	0.75	0.63	0.27	0.84	0.69	0.19	0.71	0.73	0.33			
BUI+DC							0.84	0.72	0.21	0.71	0.73	0.32			
FWI+BUI+DC										0.70	0.72	0.37			
FWI+DMC+DC										0.71	0.72	0.37			

The AUC, recall (threshold: 0.5) and false positive rate (FPR; threshold: 0.5) metrics for logistic regression prediction models by variable combination and biome–season group. The highest AUC and recall values and lowest FPR values are in bold. The best models, determined by both AUC (the most important criterion) and recall (secondary criterion), are highlighted with a red background.